Neuron
Article

Odor Representations in Olfactory Cortex: Distributed Rate Coding and Decorrelated Population Activity

Keiji Miura,[1,2,3] Zachary F. Mainen,[4,5] and Naoshige Uchida[1,5,*]
[1]Center for Brain Science, Department of Molecular and Cellular Biology, Harvard University, Cambridge, MA 02138, USA
[2]Precursory Research for Embryonic Science and Technology (PRESTO), Japan Science and Technology Agency (JST), Kawaguchi 332-0012, Japan
[3]Graduate School of Information Sciences, Tohoku University, Sendai 980-8579, Japan
[4]Champalimaud Neuroscience Programme, Champalimaud Center for the Unknown, 1400-038 Lisbon, Portugal
[5]Cold Spring Harbor Laboratory, Cold Spring Harbor, NY 11724, USA
*Correspondence: uchida@mcb.harvard.edu
DOI 10.1016/j.neuron.2012.04.021

SUMMARY

How information encoded in neuronal spike trains is used to guide sensory decisions is a fundamental question. In olfaction, a single sniff is sufficient for fine odor discrimination but the neural representations on which olfactory decisions are based are unclear. Here, we recorded neural ensemble activity in the anterior piriform cortex (aPC) of rats performing an odor mixture categorization task. We show that odors evoke transient bursts locked to sniff onset and that odor identity can be better decoded using burst spike counts than by spike latencies or temporal patterns. Surprisingly, aPC ensembles also exhibited near-zero noise correlations during odor stimulation. Consequently, fewer than 100 aPC neurons provided sufficient information to account for behavioral speed and accuracy, suggesting that behavioral performance limits arise downstream of aPC. These findings demonstrate profound transformations in the dynamics of odor representations from the olfactory bulb to cortex and reveal likely substrates for odor-guided decisions.

INTRODUCTION

Active sampling is an important component of sensory processing that can result in chunking of information into short, discrete epochs of a fraction of a second, as exemplified by visual fixations. In olfaction, rodents exhibit rapid stereotyped respiration at theta frequency (called sniffing) during active exploration (Wachowiak, 2011; Welker, 1964). Behavioral experiments have shown that a single rapid sniff can support accurate odor discrimination (Uchida and Mainen, 2003; Wesson et al., 2008), suggesting that each sniff generates a relatively complete "snapshot" of an olfactory world, and constitutes a unit of odor coding (Kepecs et al., 2006). Despite these observations, however, how sensory information is represented on this timescale and how it is transformed in the brain to ultimately control behavior remain unclear.

Studies in the olfactory bulb, the first relay in the olfactory neural pathway, have shown that odor stimulation triggers diverse temporal patterns of activity at the level of the olfactory nerve inputs and mitral/tufted cells, the exclusive outputs of the olfactory bulb (Cang and Isaacson, 2003; Friedrich and Laurent, 2001; Hamilton and Kauer, 1989; Junek et al., 2010; Macrides and Chorover, 1972; Margrie and Schaefer, 2003; Meredith, 1986; Spors and Grinvald, 2002; Wehr and Laurent, 1996; Wellis et al., 1989). During sniffing, spiking activity of mitral/tufted cells show diverse and reliable temporal patterns at the resolution of tens of milliseconds (Carey and Wachowiak, 2011; Cury and Uchida, 2010; Shusterman et al., 2011). These dynamic response patterns, in particular, those in the initial portion of the response (~100 ms), convey substantial odor information compared to the total spike counts contained in the entire period of a theta sniff cycle (Cury and Uchida, 2010), suggesting that timing of spikes plays a critical role in rapid and accurate odor coding in the olfactory bulb.

Compared to the olfactory bulb, relatively little is known about how odor information is coded by neurons in the olfactory cortex. Neurons in the olfactory bulb project broadly to the cortex without apparent topography (Ghosh et al., 2011; Miyamichi et al., 2011; Nagayama et al., 2010; Ojima et al., 1984; Sosulski et al., 2011) and odor stimulation activates widely distributed neurons in the cortex again without apparent topography (Illig and Haberly, 2003; Rennaker et al., 2007; Stettler and Axel, 2009), suggesting that the olfactory cortex might use a different mechanism for odor coding than the olfactory bulb. To elucidate coding principles in the olfactory cortex that underlie rapid olfactory decisions, here we examined (1) how active sniffing shapes neural responses, (2) whether spike times or rate carry more information, and (3) the nature of odor coding at the ensemble level. We show that odor inhalation triggers a transient burst of spikes time-locked to inhalation onset. In contrast to the olfactory bulb, timing of spikes conveyed little additional information compared to the total spike counts, demonstrating a profound transformation of coding mechanisms between the olfactory

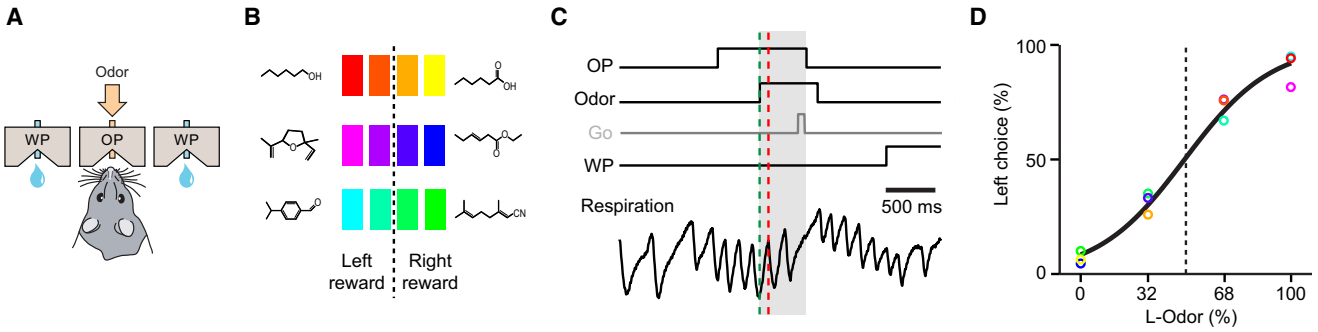

Figure 1. Odor Mixture Categorization Task and Behavioral Performance

(A and B) Schematic of odor mixture categorization task. Rats were trained to respond to the left or right reward port depending on the dominant component in a mixture. Task difficulty was varied by changing ratios of two odorants of a given odor pair (A/B: 0/100, 32/68, 68/32, 100/0). Three pairs of odors were used and all the stimuli were randomly interleaved in a session. Odors are indicated by colors: yellow, caproic acid; red, 1-hexanol; blue, ethyl 3-hexenoate; magenta, dehydroxy linalool oxide; green, citralva; cyan, cumin aldehyde. Intermediate colors represent binary mixtures of the pure odors.

(C) Task timing and respiration patterns. An odor was delivered in the odor port upon entry with a pseudorandom delay of 0.2–0.5 s. In a self-paced version of the task (reaction time paradigm, black line), rats were allowed to respond as soon as they decided to leave the port. In the go-signal paradigm, rats had to wait until a tone (go-signal, gray line) is played 700 ms after odor onset. Respiration patterns were monitored using a temperature sensor in the nasal cavity (the voltage signal from a nasal thermocouple). The gray shading indicates the timing of odor sampling.

(D) Psychometric curve. The behavioral performance for the 12 odors (same color code as A) were fitted by a sigmoid curve as a function of mixture ratio. Task performance accuracy was higher for pure compared to mixture stimuli.

See also Figure S1.

bulb and cortex. Furthermore, odor stimulation reduced correlated noise among neurons, which facilitated the efficiency of population coding in the olfactory cortex.

RESULTS

We recorded spiking activity of olfactory cortical neurons in rats while simultaneously monitoring their sniffing and performance in a two-alternative choice odor mixture categorization task (Uchida and Mainen, 2003; Figure 1A). The stimuli consisted of three or four odor pairs with each odor delivered either alone (100/0, 0/100) or in mixtures (68/32, 32/68) (Figure 1B). All stimuli were randomly interleaved and one odor of each pair was assigned to the right and the other to the left choice port, with mixtures rewarded according to the dominant component. One set of subjects (n = 5) performed a reaction time version of the task, taking one to two sniffs between odor onset and response initiation (1.71 ± 0.01; see Figure S1B available online; Uchida and Mainen, 2003). A second set of subjects (n = 3) was trained to wait for a tone (Rinberg et al., 2006) at 700 ms delay from odor valve onset in order to enforce a longer odor sampling period (Figure 1C) and more sniffs (3.84 ± 0.03, $p < 0.05$ compared to reaction time paradigm; Figure S1B). In both paradigms, rats sniffed at theta frequency during odor sampling (7.18 ± 0.29 and 6.35 ± 0.27 s^{-1}, respectively; Figure 1C). Task performance accuracy was higher for pure than mixture stimuli across all pairs, but was independent of the training paradigm and of the number of sniffs taken within a given paradigm (Figures 1D, S1C, and S1D). Thus, as previously reported (Uchida and Mainen, 2003), a single sniff was sufficient for maximal performance by rats in this odor mixture categorization task.

We recorded from ensembles of up to 21 neurons (9.4 ± 4.7, mean ± SD) in the anterior piriform cortex (aPC) using chronically implanted tetrodes during performance of the above tasks (see Experimental Procedures for details). From a total of 460 well-isolated single neurons, 179 neurons recorded using a fixed panel of 6 odorants formed the primary data set for the subsequent analyses. Given the similarity of behavioral performance in reaction-time and go-signal paradigms, data from these experiments was pooled (91 neurons from the reaction time paradigm and 88 neurons from the go-tone paradigm).

Sniffing of Odors Triggers Transient Spike Bursts Tightly Locked to Inhalation Onset

Previous studies have noted relatively brief, burst-like responses in PC (McCollum et al., 1991; Wilson, 1998), but these studies did not explicitly compare neural responses with respiration. We found that odor responses in aPC consisted typically of a transient burst of spikes time-locked to the onset of odor inhalation. Aligning spike times relative to the onset of the first sniff after odor onset revealed a much tighter temporal organization than was apparent by aligning on odor valve opening (Figures 2A–2C). Indeed, some responses were detectable only using sniff locking (Figures S2A and S2B). Responses peaked rapidly (T_{peak}: 99 ± 45 ms from the first inhalation onset, median ± SD; Figure 2D) and returned to baseline rapidly (full-width at half max: 32 ± 24 ms, median ± SD; Figure 2E). Thus, odor-evoked transients lasted approximately one sniff cycle (158.1 ± 40.2 ms, mean ± SD).

Odor Stimulation Evokes Broadly Distributed, Moderately Sparse Ensemble Neurons

Single neurons in aPC showed robust and stimulus-specific responses to odor stimuli (Figure 3A). Relatively little selectivity for spatial choices (left versus right) or reward outcomes was observed (Figure 3B). As a population, 45% of aPC neurons

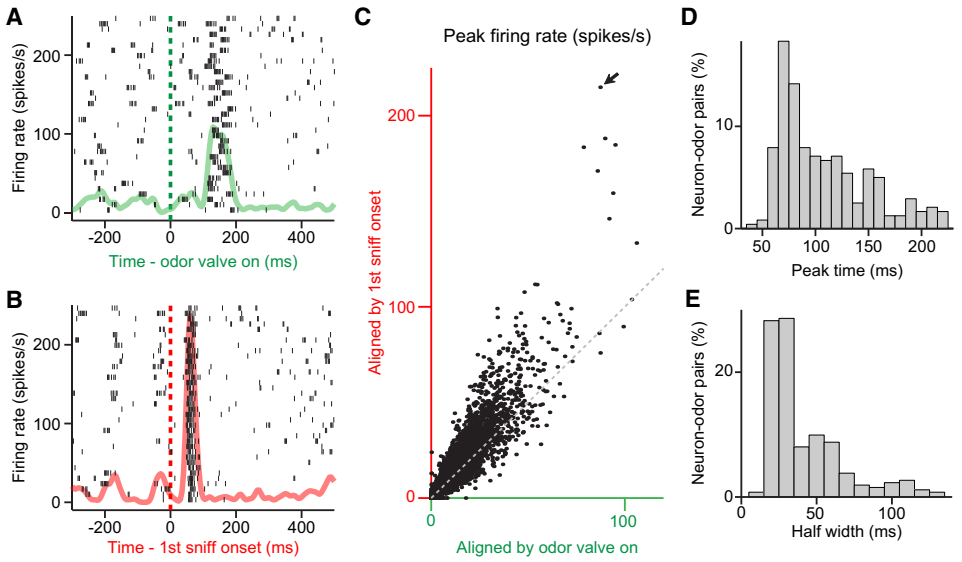

Figure 2. Sniffing of Odors Triggers Transient Spike Bursts Tightly Locked to Inhalation Onset

(A and B) Activity of an example aPC neuron. Raster plots represent neural activity with each row corresponding to a single trial (n = 37 trials) and each tick mark to a spike. Peri-event histograms are overlaid (green and red, smoothed with a Gaussian filter with the standard deviation of 7.5 ms). Trials are aligned to onset of odor valve opening (A) or first sniff after odor valve opening (B). In (B), periodic spontaneous activity before t = 0 that reflects sniffing is evident.

(C) Comparison of peak firing rates between the two alignment conditions (odor valve opening versus first sniff onset). Instantaneous firing rates were calculated after smoothing the peri-event histogram using a Gaussian filter (SD: 7.5 ms). The arrow denotes the example in this figure (A and B). A baseline firing rate (0 to 0.5 s before odor valve onset) was subtracted for each neuron-odor pair. The peak firing rates are higher when triggered by the first inhalation onset ($p < 10^{-10}$, Wilcoxon signed-rank test).

(D) Histogram of peak timing. Data from 243 odor-responsive neurons.

(E) Histogram of temporal half width of peak firing. Same data as in (D).

See also Figure S2.

were activated by at least one of the six odors tested while 28% were activated by two or more (Figures 3C, 3D, and S3; $p < 0.05$, Wilcoxon rank-sum test). Conversely, each odor caused significant responses in 16.5% ± 3.1% of aPC neurons (mean ± SD, n = 6 odors, 10.3% excitatory, 6.2% inhibitory). The probability of response of a piriform neuron to an odor was well-fit by a binomial distribution with an extra allowance for nonresponding neurons (Figure 3D). We calculated a population sparseness of 0.41 and a lifetime sparseness of 0.61 (see Experimental Procedures), somewhat lower than previously observed in aPC of anesthetized rats (Poo and Isaacson, 2009). Therefore, aPC responses were observed in broadly distributed, moderately sparse neural populations, largely consistent with previous studies (Poo and Isaacson, 2009; Rennaker et al., 2007; Stettler and Axel, 2009; Zhan and Luo, 2010).

Spike Counts Carried More Reliable and Rapid Information Than Temporal Patterns

The latency and peak timing of aPC responses varied across neurons and odors, raising the possibility that these parameters may carry odor information (Cury and Uchida, 2010; Figures 4A and 4B). However, both of these timing parameters were anti-correlated with spike counts (Figures 4C and 4D), suggesting that the information conveyed by these variables might be redundant. In order to quantify the amount of information carried by different response variables (i.e., latency, peak timing and spike counts), we performed a decoding analysis to ask how accurately an ideal observer could classify each individual trial as belonging to one of six odor stimuli. By comparing decoding accuracy using vectors consisting of different variables derived from aPC responses, we compared the relative importance of each coding strategy. As decoders (ideal observers), we used linear classifiers including perceptrons and support vector machines with linear kernels. These decoders essentially calculate a weighted sum of inputs followed by a threshold and therefore resemble a biophysical decoding of aPC information that might actually be implemented in downstream areas.

Input codes based on the total number or rate of spikes in a sniff cycle provided the most reliable performance in odor classification, whereas codes based on first spike latency or peak timing performed significantly worse (Figure 4E). Furthermore, combining latency or peak timing with rate failed to improve decoding accuracy. Although it has been postulated that spike times may provide a more rapid coding mechanism (Cury and Uchida, 2010; Gollisch and Meister, 2008; Thorpe et al., 2001), we found that decoders using spike count actually performed faster than those based on spike latency or peak timing (Figure 4F), demonstrating that spike counts can convey information both more quickly and in a more reliable manner. Furthermore, decoding based on complete temporal patterns of activity in a sniff cycle did little to improve decoding accuracy (Figure 4G). Finally, using phase of spike occurrence with

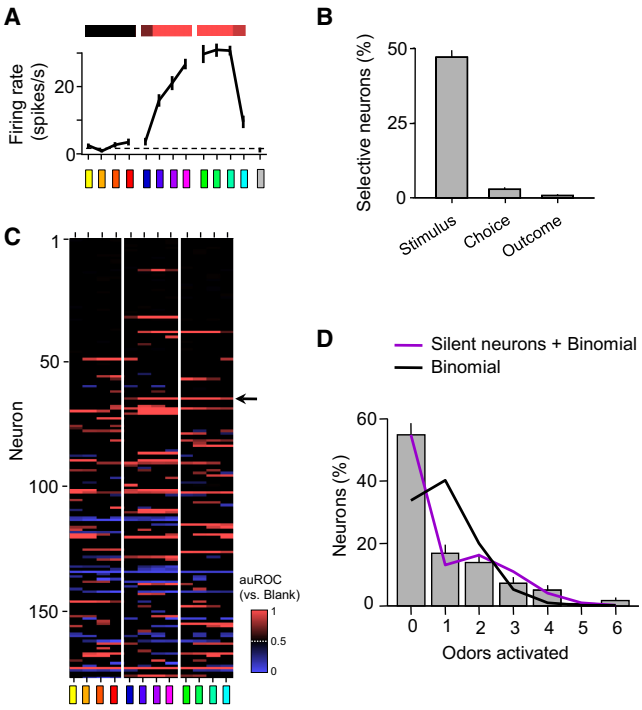

Figure 3. Moderately Sparse, Distributed Population Odor Responses in aPC

(A) Odor-evoked responses of an example neuron during first sniff cycle after odor onset. The bottom colors indicate odors tested (same colors as in Figure 1B). The middle plot shows the firing rates in first sniff after odor valve opening (40–160 ms from inhalation onset) as a function of odor stimuli. The dashed line indicates the firing rate at the preodor sniff. The top colors indicate the magnitude of odor response to each stimulus. The response magnitudes were calculated as a comparison with blank (no odor) trials using signal detection analysis (area under the receiver operating characteristics curve, auROC; see Experimental Procedures). Scale is shown in (C) (red: excitatory response with perfect discriminability, black: no discriminability [no response], blue: inhibitory response with perfect discriminability).

(B) Statistical analysis of neural activity during first sniff (40–160 ms window from sniff onset) (three-way ANOVA performed for each neuron with factors of stimulus identity, choice direction and reward outcome, $p < 0.05$). Neural responses during this period mostly reflect odor stimuli but not behavioral choice or reward outcomes.

(C) Summary of odor responses (179 neurons). Odor response magnitudes were indicated as in (A), top (also see color scale). Nonsignificant responses ($p > 0.05$, Wilcoxon rank-sum test) are shown in black. The example neuron in (A) is indicated by the arrow. Neurons are sorted by preodor firing rates in an increasing order.

(D) Histogram of number of pure odorants that activated a given neuron ($p < 0.05$, Wilcoxon rank-sum test). Two lines represent binomial fits with (purple; nonresponsive $p_0 = 0.50$, the other neuron respond with $p = 0.16/(1-p_0) = 0.33$) or without allowance of extra nonresponsive neurons (orange; $p = 0.16$). As a population, 45% of aPC neurons were activated by at least one of the six odors tested while 28% were activated by two or more (<0.05, Wilcoxon rank-sum test).

See also Figure S3.

respect to sniffing cycle instead of absolute time did not improve the decoding accuracy (Figure 4H). Together, these results suggest that spike rates or counts are the predominant carrier of olfactory information in the aPC, and that the dependence of odor coding on spike timing is greatly reduced compared to the olfactory bulb (Cury and Uchida, 2010).

Information Conveyed by the Spike Counts Provided in Burst Activity Can Account for the Speed and Accuracy of Odor Discrimination

We next compared the performance of aPC populations decoded using linear classifiers to the performance of the animal. Decoding based on total spike counts in the first sniff using the entire 179 neurons gave nearly perfect performance on pure odors (Figures 5A and 5B). For both pure and mixture stimuli, the accuracy of the classifier reached a level comparable to that of the animal using only about 70 neurons (Figure 5A). Analysis of the time course of decoding using a short sliding time window showed that the maximum information could be read out from the initial burst of activity within 100 ms after the first inhalation onset and that the rate of information dropped thereafter (Figures 5B and 5C). Comparing the first and second sniff separately, spikes in the first sniff gave significantly higher accuracy than those in the second sniff or the last sniff before odor port exit (Figure 5D; $p < 0.05$, χ^2 test), and using both the first and second sniff cycles resulted in only a small increase in accuracy (Figure 5D). Therefore, spike counts in ensembles of aPC neurons appear to be sufficient to explain both the speed and accuracy of decisions in an odor mixture discrimination task.

Spike Counts in Ensemble Activity Correlate with Behavioral Choices

If firing rates across ensembles of aPC neurons are used by the brain to form behavioral responses, and if sensory uncertainty reduces performance accuracy, as in the mixture trials, then we might be able to observe trial-by-trial correlations between decoding based on these neural representations and the animals' choices. To test this idea, we first compared neuronal firing rates on correct and error choices for a given stimulus, a measure analogous to "choice probability," a measure that has been used previously to test the role of a neural representation in behavior (Britten et al., 1996; Cury and Uchida, 2010; Parker and Newsome, 1998). We found a low average correlation between the firing rates of individual neurons and subjects' choices (avg. choice prob. = 0.51 ± 0.011; Figures 5E and 5F). This correlation was somewhat smaller than those found in previous observations in visual cortex (0.53–0.7; Britten et al., 1996; Cohen and Newsome, 2009; Dodd et al., 2001; Uka and DeAngelis, 2004). However, if the information for choices is distributed across a large number of uncorrelated aPC neurons such that the contribution of single neurons is diluted (Cohen and Newsome, 2009), then we reasoned that the accuracy of decoding based on simultaneously recorded ensembles may be correlated on a trial-by-trial basis with behavioral choices. Indeed, we found that patterns of spike counts across aPC neurons in correct trials provided significantly higher decoding accuracy than patterns in error trials (Figure 5G; $p = 0.030$, Wilcoxon test). In contrast, decoding using peak timing or latency did not show a significant difference between correct and error trials (Figures 5H and 5I; $p > 0.05$, Wilcoxon test). Therefore, spike rates in aPC not only carry substantial stimulus

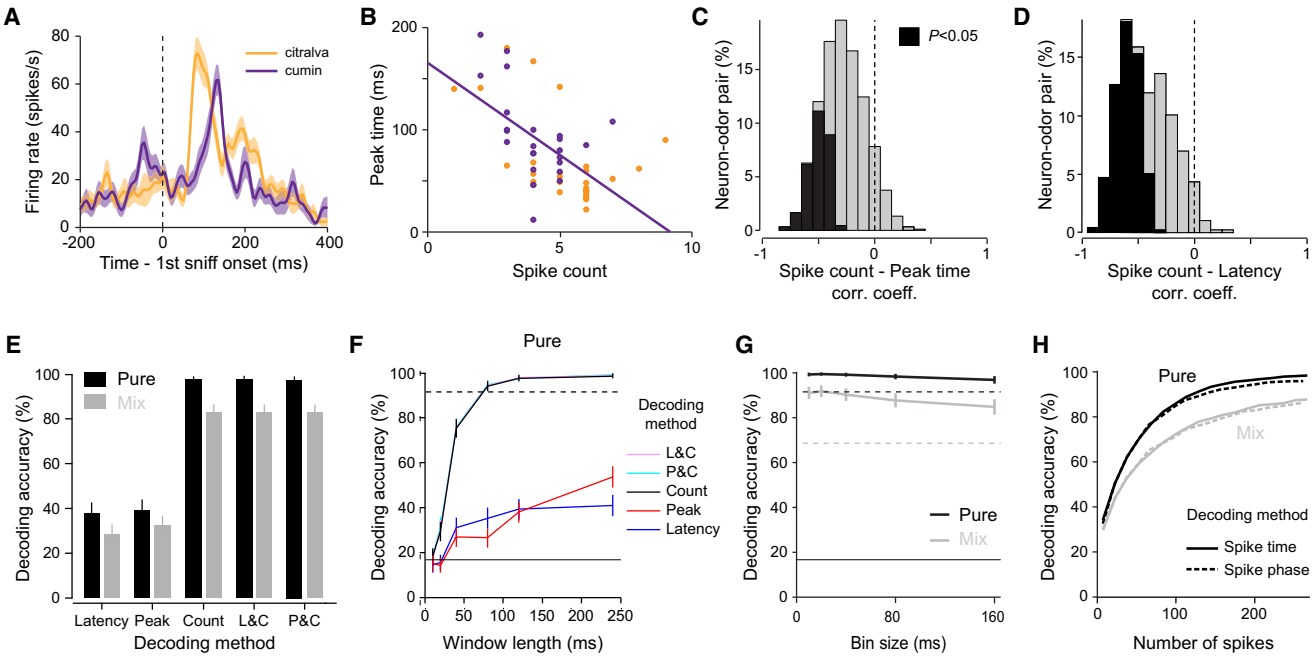

Figure 4. Rapid and Accurate Readout of Odor Information Based on Spike Counts in First Sniff

(A) Activity of an example neuron in response to two different odors. This neuron responded to the two odors with different temporal profiles.

(B) Trial-to-trial relationship of peak timing and total spike counts (same neuron and odors as in A). Each dot corresponds to one trial. Peak time is defined as the time when the smoothed firing rate profile reaches the maximum firing rate within the first sniff cycle.

(C and D) Correlation coefficients between spike counts and peak timing (C) and latency (D) for 908 neuron-odor pairs. Black bars indicate significant correlations ($p < 0.05$).

(E) Odor decoding accuracy of a linear decoder based on different firing features. Information contained in ensemble neural activity (179 neurons) in one sniff (40–160 ms from inhalation onset) was quantified by the accuracy with which a linear classifier (support vector machine with a linear kernel) can correctly identify one out of six odors on a trial-by-trial basis (see Experimental Procedures). Decoding accuracy for six pure odors (black) and six odor mixtures (gray) are plotted separately. Latency: time of first spike. Peak: time of peak firing rate. Count: total spike count. L&C: latency and spike count. P&C: peak time and spike count.

(F) Odor decoding accuracy with increasing window lengths. Decoding using peak timing does not result in any faster performance than that using only spike counts. A total of 179 neurons are used. The decoding is based on trials with pure odors. Chance performance level is 16.67% (=1/6, horizontal thin line). Black horizontal dashed line indicates the behavioral performance level for pure odors. Three curves (L&C, P&C, and Count) are highly overlapping.

(G) Odor decoding accuracy of a linear classifier, plotted as a function of bin size (10 ms to 160 ms, i.e., temporal resolution). A 160ms time window after the first sniff was first equipartitioned into smaller sized bins (80, 40, 20, or 10 ms, respectively) and then the spike counts in all the bins were used for classification. Black, pure; gray, mixture stimuli. Black and gray horizontal dashed lines indicate the behavioral performance levels for pure and mix odors, respectively.

(H) Odor decoding accuracy based on spike counts and phases for pure and mixture trials. Spike time: spike counts in 160 ms × 1 bin. Phase: spike counts in eight bins equipartitioning the first sniff cycle. Note that bin widths vary by trials in Phase. For fair comparisons, decoding accuracy was plotted against the mean number of spikes per trial instead of the number of neurons.

information, they are also correlated at an ensemble level with the behavioral choices of the animal.

Near-Zero Noise Correlations during Odor Inhalation

The above results indicate that odor information is coded by a large number of neurons in aPC. A critical feature of information coding in neuronal ensembles is the structure and magnitude of correlated fluctuations in firing, which can affect the ability of downstream neurons to decode the information. A simple example of ensemble decoding is population averaging or pooling. By this strategy, neuronal noise can, in principle, be eliminated by averaging the activity of a large number of neurons. However, if noise is not random across neurons, that is, if neural activity cofluctuates across neurons, the benefit of pooling can be significantly curtailed (Cohen and Kohn, 2011; Zohary et al., 1994). The choice probability analysis suggested that aPC neurons are actually very weakly correlated. To test more directly whether such correlations affect representations of odors in the olfactory cortex, we analyzed the "noise correlations" between pairs of simultaneously recorded aPC neurons (see Experimental Procedures). Noise was defined as the trial-to-trial variability of spike counts in a sniff cycle (40–160 ms after the first sniff onset) around the mean response under a given stimulus condition. Noise correlation was defined as the correlation coefficient between the noise of two neurons to multiple presentations of a given odor stimulus. We found surprisingly low noise correlations among aPC neurons (0.0046 ± 0.0988; mean ± SD; n = 936 pairs; Figures 6A and S5). In fact, both the mean and the standard deviation of noise correlations of the aPC data were similar to trial-shuffled data in which all correlations are removed (0.00011 ± 0.0870; Figures S5C–S5F), suggesting that deviations from zero were mostly due to the effect of finite sample size

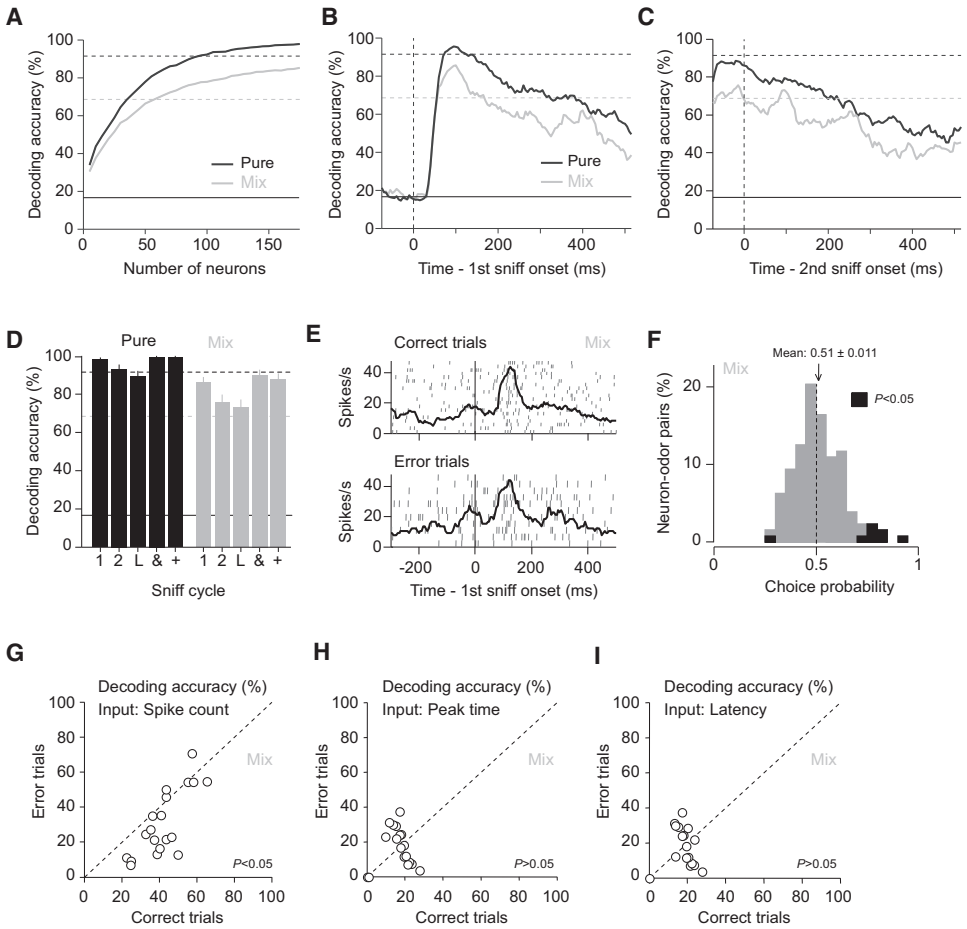

Figure 5. Information Conveyed by the Spike Counts in the Burst Activity Can Account for the Speed and Accuracy of Odor Discrimination

(A) Decoding accuracy as a function of the number of neurons. Total spike counts within 40–160 ms after the first sniff onset were used. Black: pure; gray: mixture stimuli. Dashed lines indicate behavioral performance levels.

(B) Time course of odor decoding accuracy. A vector consisting of instantaneous spike counts of 179 neurons in a sliding window (width, 50 ms; step, 5 ms) was used for the input to a classifier. Training of the classifier and testing were done at every time point.

(C) Time course of odor decoding accuracy after the second sniff onset.

(D) Odor decoding accuracy at different sniff cycles. 1, first sniff; 2, second sniff; L, last sniff before odor port exit. +, sum of the spike counts from first and second sniffs. &, spike counts from the first and second sniffs are treated as independent inputs to a classifier. Note that the last sniffs contain first or second sniff depending on how many sniff the animal took in a given trial. The neural response at the first sniff is more informative than the second and the last sniffs. Combining first and second sniffs improved decoding accuracy only a little (statistically not significant either for pure or mixture odors, $p > 0.05$, χ^2 test).

(E) Comparison of the responses of an example neuron to the same odor on correct trials and error trials.

(F) Choice probabilities: correlations between a trial-to-trial variability in neural activity and a choice toward neuron's preferred direction. Only mixture odor trials were used to obtain a larger number of error trials. The fraction of neurons with significant choice probabilities >0.5 is significantly larger than the fraction with significant choice probabilities <0.5 ($p < 0.05$, χ^2 test) although the mean choice probability was not significantly larger than 0.5 (Wilcoxon sign-rank test, $p > 0.5$). A neuron's preferred choice direction was determined as a direction for a pure odor with significantly higher firing rate than the paired pure odor. Only neuron-mixture odor pairs where two pure odors showed significantly different responses (area under receiver operating characteristic curve >0.7 or <0.3) and with numbers of trials for each choice more than five were used for the analysis.

(G–I) Odor decoding accuracy for correct and error trials using simultaneously recorded ensemble neurons (n = 19 sessions). Total spike counts within 40–160 ms (G), Peak time (H) and latency (I) from the first sniff onset were used. Only trials with mixture odors, where most of error trials are available, were used. A classifier was first trained using correct trials, and decoding accuracy was obtained using test trials that are composed of correct or error trials. $p < 0.05$ for spike counts (Wilcoxon test).

See also Figure S4.

(Ecker et al., 2010). Moreover, we observed no dependence of the magnitude of noise correlations on the number of evoked spikes over a range of rates <5 to >100 spikes • s^{-1} (Figures S5A and S5B). Therefore, near-zero noise correlations in aPC were not a consequence of low firing rates (Cohen and Kohn, 2011; de la Rocha et al., 2007; Kohn and Smith, 2005).

In the neocortex, neighboring neurons with similar stimulus tuning tend to exhibit correlated trial-by-trial fluctuations in firing

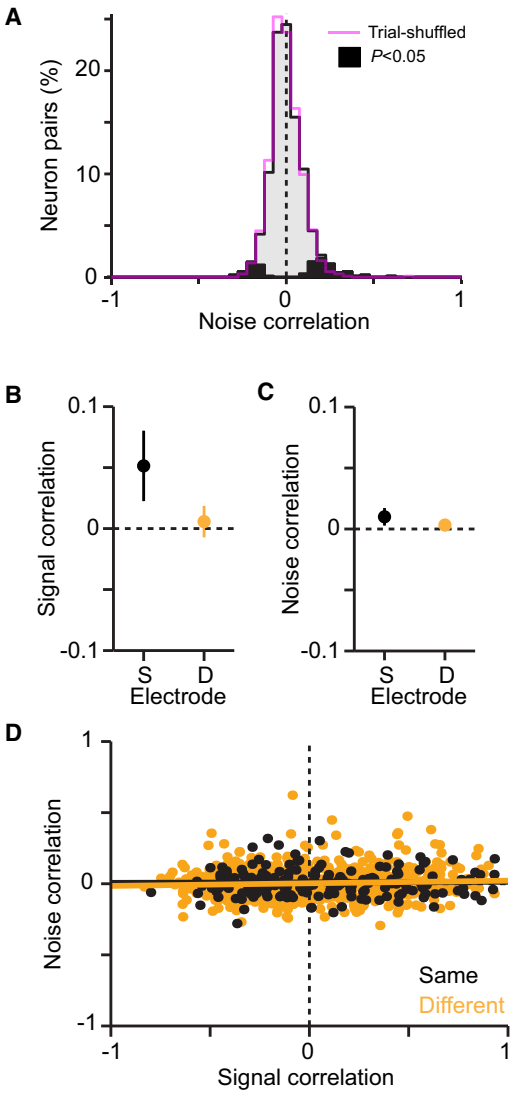

Figure 6. Near-Zero Noise Correlations in aPC

(A) Histogram of noise correlations. Noise correlations were calculated using spike counts in the first sniff cycle after odor onset (40–160 ms). A similar distribution of noise correlations was obtained after trial-shuffling (magenta), indicating that most neuron pairs had zero noise correlations. Black bars indicate correlations significantly different from zero ($p < 0.05$).

(B) Signal correlations (similarity in odor response tuning for a pair of neurons) compared between neuron pairs from same (S) and different (D) electrodes. Neuron pairs from same electrode showed slightly higher signal correlations ($p > 0.05$, Wilcoxon rank-sum test). The error bars are SEM across neuron-odor pairs.

(C) Noise correlations compared between neuron pairs from same and different electrodes. There was no difference in noise correlations ($p > 0.05$, Wilcoxon rank-sum test). The error bars are SEM across neuron-odor pairs.

(D) No dependency between noise correlations and signal correlations. Neuron pairs recorded from same (S) and different (D) electrodes are indicated by black and orange dots, respectively. Neither the slope nor intercept of the regression lines were significantly different from 0 (red and black lines, $p > 0.05$, linear regression), indicating no relationship between noise correlations and signal correlations.

See also Figure S5.

rate (Bair et al., 2001; Cohen and Kohn, 2011; Zohary et al., 1994), thought to arise from common inputs, and it has been postulated that these "structured" or "limited-range" correlations are particularly detrimental to the efficiency of population coding (Averbeck et al., 2006; Sompolinsky et al., 2001). We therefore examined whether noise correlations between aPC neurons are low even when their odor tuning is similar. To quantify the similarity of odor tuning between pairs of neurons, we calculated the correlation coefficient of the mean odor responses across all 12 stimuli used (i.e., signal correlation). This analysis showed that signal correlations were low both for aPC neurons recorded on the same tetrode and for those recorded on different tetrodes ($p > 0.05$, Wilcoxon rank-sum test; Figure 6B). Similarly, noise correlations were near-zero regardless of whether neurons were recorded on the same or different tetrodes ($p > 0.05$, Wilcoxon rank-sum test; Figure 6C). Most importantly, the noise correlations of pairs of aPC neurons were independent of their signal correlations (regression slope: 0.0156 ± 0.0090, not significantly different from zero, $p > 0.05$; Figure 6D). These results suggest that, during odor stimulation, aPC neurons act largely as independent encoders regardless of their distance or the similarity of their odor tuning.

Odor Inhalation Quenches Noise Correlations

Neuronal variability and noise correlation are not static, but can be modulated by attentional state (Cohen and Maunsell, 2009; Mitchell et al., 2009), perceptual learning (Gu et al., 2011), and stimulus input (Bhandawat et al., 2007; Churchland et al., 2010; de la Rocha et al., 2007; Kazama and Wilson, 2009). Therefore, in order to gain insight into how near zero noise correlations arise in aPC, we tested how trial-to-trial correlations across neurons are modulated during the course of events in each trial. For this analysis, since odor stimuli were not always present, we calculated the correlation coefficients of spike counts without subtracting the mean responses of each stimulus condition (see Experimental Procedures for more details). We found that when rats begin active sampling (sniffing) in anticipation of odor presentation, the aPC population was globally activated, with the mean population firing rate increasing by around 30% (Figure 7A). Surprisingly, during the same period the mean pairwise correlation across the entire population dropped, implying a possible positive impact on population coding (Zohary et al., 1994). However, correlations between similarly tuned pairs increased (Figures 7B–7D and S6A–S6C; regression slope, 0.0916 ± 0.0092, significantly different from zero, $p < 0.01$), implying a possible negative impact on population coding (Sompolinsky et al., 2001). In order to estimate the net effect, we performed decoding analysis using simulated data in which spike counts obtained during odor stimulation were trial-shuffled to generate noise correlation structures with different means and signal correlations while preserving the mean odor response profile of individual neurons (see Experimental Procedures for details). We found that correlations of the type observed during the pre-odor-sampling period, had they persisted into the odor-sampling period, would have significantly eroded the efficacy of decoding, reducing classifier performance by more than 5%–10% ($p < 0.01$, t test; Figures 8A–8C and S7). We calculated that 2–3 times more neurons would have been required to

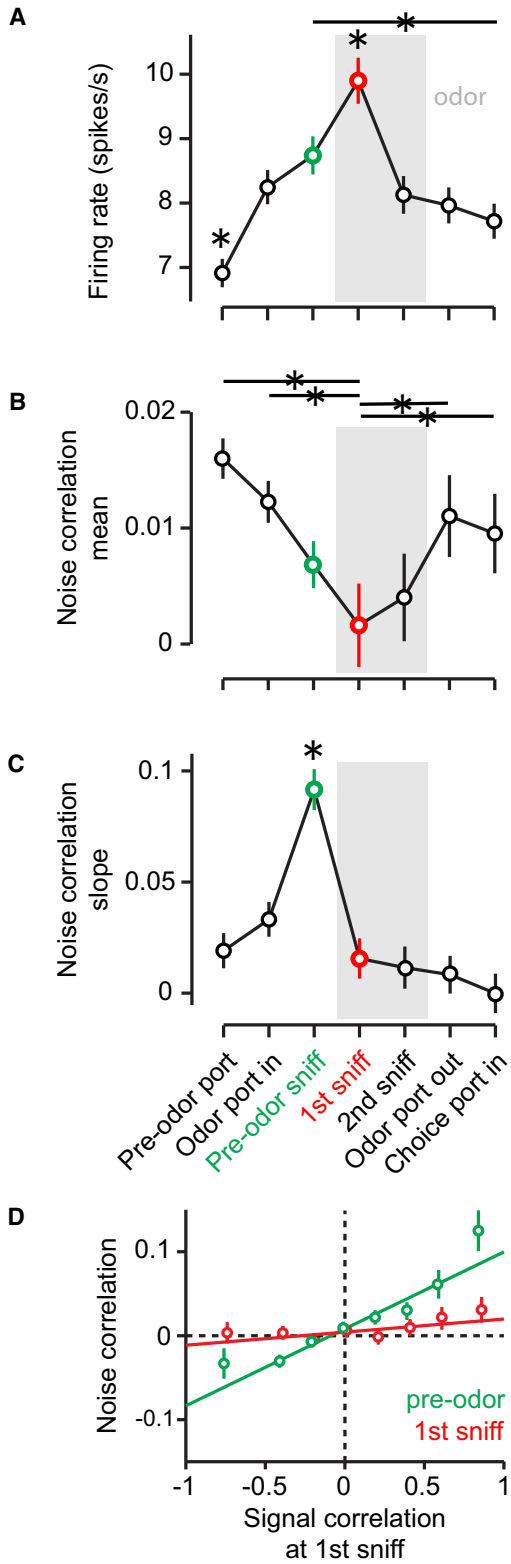

Figure 7. Odor Stimulation Quenches Structured Trial-to-Trial Correlations that Emerge during Preodor Sniffing

(A) Mean firing rate over the population as a function of task epochs. Spikes in the first sniff after each task event were used. Preodor port: 500 ms before odor port in. A bar with a star indicates significance between two epochs and a star without a horizontal bar indicates the significance against all the other epochs (the error bars are across neuron-odor pairs, ANOVA with LSD method).

(B) Mean correlation as a function of task epochs. The error bars are for neuron-odor pairs.

(C) Regression slopes for the trial-to-trial correlation and signal correlation relationship as a function of task epochs. Trial-to-trial correlations were computed at each epoch while signal correlations were computed at the first sniff (generalized linear model with Holm method). The error bars are SEM across neuron-odor pairs.

(D) Trial-to-trial correlations as a function of signal correlations. Two task epochs, preodor (green) and first sniff (red), are plotted separately ($p < 0.05$ for slopes, generalized linear model). The error bars are SEM across neuron-odor pairs.

See also Figure S6.

achieve the same level of decoding performance had pre-odor correlation levels been maintained (Figure 8D). The simulation also indicated that the effects would be even larger with larger ensembles. We also found that trial-to-trial variability in spike count, as measured by the Fano factor and the coefficient of variation, was significantly reduced by odor onset (Figures S6D and S6E). Thus, potentially deleterious population correlations are increased during the period of high sniffing preceding odor onset but these correlations are quenched during the arrival of the stimulus (Churchland et al., 2010).

DISCUSSION

Transformation of Odor Representation between the Olfactory Bulb and Piriform Cortex

Together with recent studies of neural coding in the olfactory bulb (Carey and Wachowiak, 2011; Cury and Uchida, 2010; Shusterman et al., 2011), this study demonstrates that odor representations are profoundly transformed between the bulb and the aPC. While these studies show that odor responses in the olfactory bulb exhibit complex temporal patterns carrying stimulus information, here, we show that those in the aPC consist primarily of a simple burst of firing, locked to respiration. Furthermore, the baseline firing rates are higher in the olfactory bulb compared to the piriform cortex (12.9 ± 6.4 Hz in the olfactory bulb; 6.15 ± 9.01 Hz in the aPC; mean ± SD; Cury and Uchida, 2010, and the present study). As a consequence, whereas in the olfactory bulb extracting information from mitral/tufted cells requires decoding of temporal patterns (Cury and Uchida, 2010), in the aPC most odor information can be read out using only spike counts of neurons.

Why might the olfactory bulb and cortex areas use different strategies for odor coding? One important consideration is the substantial anatomical differences between the two areas: while a relatively small number of neurons (20–50 mitral cells) transmit odor information from each of the approximately 1000 input channels (glomeruli) in the olfactory bulb, this information is broadcast to an olfactory cortex that contains an estimated two orders of magnitude more neurons (Shepherd, 2004). Because of this expansion in coding space the necessity to maximize the rate of information transmitted per neuron and per unit time in the olfactory bulb will be much greater than in

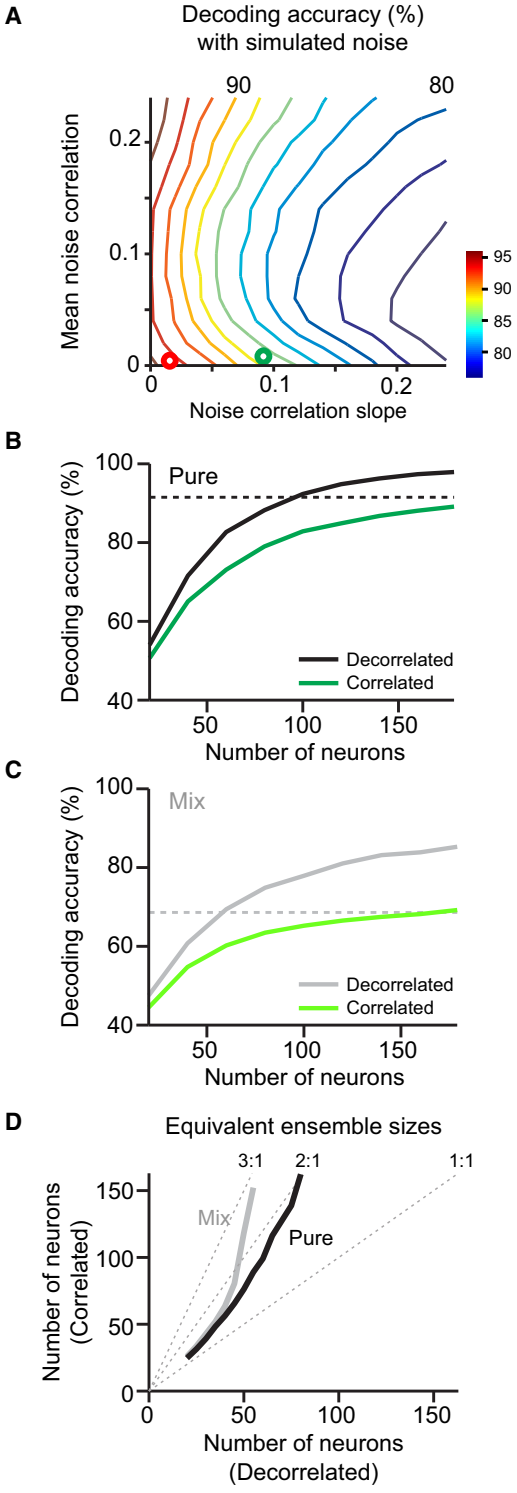

Figure 8. Odor Decoding Accuracy in the Presence of Simulated Noise Correlation Structures

(A) To simulate odor evoked activity that has an arbitorary noise correlation structure, trials were shuffled to artificially induce the mean and slope of the noise and signal correlation relationship. Shuffling was performed multiple times toward minimizing the least square error to achieve the target noise correlation structures defined by its intercept and slope. Odor-decoding accuracy was then computed using the trial-shuffled ensemble activity. The green and red circles indicate preodor and first sniff, respectively.

(B and C) Decoding accuracy using decorrelated (black, gray) and correlated ensembles (green, light green) as a function of number of neurons. Pure (B) and mixture (C) odors were plotted separately. The mean and slope of the correlations observed during the pre-odor period were used to simulate correlated ensembles. The dashed lines denote the animals' behavioral performance for each condition. The decorrelated ensemble results are the same as in Figure 5A.

(D) Equivalent ensemble sizes. The number of neurons required to achieve the same decoding accuracy between decorrelated and correlated ensembles were obtained from (B) and (C). The dotted lines represent ratios (3:1, 2:1, 1:1) of the numbers of neurons between decorrelated versus correlated ensembles. As the size of a population increases, disproportionately more neurons are required to achieve the same performance in the presence of structured noise correlations.

See also Figure S7.

the aPC. The cortex can therefore better afford to employ a rate-based coding strategy based on a larger number of neurons and a widely distributed code. One significant advantage of rate-based code over temporal code is that downstream areas can more readily read out such a code or combine it with other kinds of information encoded in rates. This might then facilitate proposed functions of the piriform cortex such as forming associative memories (Franks et al., 2011; Haberly, 2001).

The mechanism of the temporal-to-rate transformation remains to be determined. In insects, temporally dynamic responses in the antennal lobe (AL, considered equivalent to the olfactory bulb) are transformed into sparse responses in the mushroom body (MB, considered equivalent to the PC). Various mechanisms have been proposed to underlie this process, including (1) oscillatory spike synchronization, (2) short membrane time constants of MB neurons, (3) feedforward inhibition, and (4) highly convergent connectivity between the AL and MB (Perez-Orive et al., 2002, 2004). In zebrafish, different mechanisms appear to shape the responsiveness of cortical neurons: neurons in the dorsal telencephalon (Dp) effectively discard information about synchronous firing in the olfactory bulb due to cortical neurons' slow membrane time constants and relatively weak feedforward inhibition (Blumhagen et al., 2011). It will be important to examine whether PC neurons in mammals are tuned to temporal patterns of activity in the olfactory bulb (Carey and Wachowiak, 2011; Cury and Uchida, 2010; Shusterman et al., 2011), and if so, which aspects of temporal patterns are important.

Neural Substrate for Rapid Olfactory Decisions

Our findings bear on the relationship between psychophysical limits and neuronal representations, a central subject in sensory physiology (Parker and Newsome, 1998). We found that, by monitoring spikes from as few as 50–100 aPC neurons, a simple decoder based on firing rates could extract more than enough information in a single sniff cycle to account for the behavioral accuracy of rats in the odor categorization task. We also found that while single neuron activity was not on average different between correct and error trials (low average "choice probability"), population activity-based decoders performed significantly better on correct compared to error trials. Rate information peaked within 100 ms during the first sniff, and

aggregating information over longer periods in multiple sniff cycles failed to significantly augment decoding performance, providing an explanation for the rapid speed of olfactory discrimination performance and the lack of speed-accuracy tradeoff over longer periods (Uchida and Mainen, 2003). Therefore, these observations provide substantial evidence linking a rate-based population code to behavioral performance.

Near-Zero Noise Correlations Facilitate Odor Coding

We found that an optimal linear decoder of aPC neurons can reach levels of performance superior to the animal itself using <100 neurons out of the estimated population of around 10^6 neurons (Shepherd, 2004). The aPC clearly contains an extremely robust representation of odor identity. What then ultimately limits behavioral accuracy? While similar observations in the visual system have attributed behavioral performance limits to the reduced efficiency of pooling in the actual network of neurons due to ensemble correlations (Shadlen et al., 1996; Zohary et al., 1994), this appears not to be the case in the aPC. During odor stimulation, aPC networks have near zero mean noise correlation, more than one order of magnitude lower than that generally reported in the neocortex (0.05–0.2; Cohen and Kohn, 2011; Gawne and Richmond, 1993; Lee et al., 1998; Zohary et al., 1994; Figure 6A), similar to that reported in the primary auditory cortex of anesthetized rats (Renart et al., 2010) and area V1 of awake monkeys (Ecker et al., 2010). More importantly, aPC neurons also lack the positive relationships between signal and noise correlations that are typically observed (Bair et al., 2001; Gu et al., 2011; Zohary et al., 1994). However, the absence of such correlations is not simply due to the distributed connectivity of the olfactory cortex: Such structured correlated activity can and does emerge prior to odor onset and simulations demonstrated that such correlations would have substantially reduced the efficiency of population coding. However, we found when driven by odor stimulation, these prestimulus correlations are quenched. While we cannot rule out the possibility that additional correlations that we were unable to measure with this data set might affect decoding, behavioral performance in the odor mixture categorization task appears to be limited neither by the level of noise of the sensory representation nor by correlated fluctuations among the population of neurons. We therefore conclude that the limits of performance must be set either by the ability of downstream circuits to accurately read out of these representations or by other non-sensory sources of variability.

Whether prolonged odor sampling can improve the accuracy of odor discrimination has been controversial. Some studies have suggested that the accuracy of odor discrimination can be improved with longer odor sampling over 500 ms (Rinberg et al., 2006) or more (Friedrich and Laurent, 2001). It has been suggested that the accuracy of discrimination of highly similar odor pairs might depend on the refinement of odor representations through temporal evolution of neural activity (Friedrich and Laurent, 2001) or through temporal integration of sensory evidence. However, the result of the present study suggests that these processes are unnecessary. These findings indicate, instead, that performance accuracy is affected not only by stimulus information but additionally by other task parameters that may affect the ability of the animal to choose accurately based on olfactory stimulus representations (H. Zariwala et al., 2005, Soc. Neurosci., abstract). It remains to be seen whether similar conclusions can be drawn in different olfactory tasks such as odor detection, discrimination at low concentrations, or more complex tasks. The present study indicates that neuronal recording in animals performing these behavioral tasks will be a critical step toward addressing these fundamental questions.

EXPERIMENTAL PROCEDURES

All procedures involving animals were carried out in accordance with NIH standards and approved by the Cold Spring Harbor Laboratory and Harvard University Institutional Animal Care and Use Committee (IACUC). All values were represented by mean ± SEM unless otherwise noted.

Behavior

Rats were trained and tested on a two-alternative choice odor mixture categorization task where water was used as a reward as described previously (Cury and Uchida, 2010; Uchida and Mainen, 2003). Odor delivery was controlled by a custom-made olfactometer (Cury and Uchida, 2010; Uchida and Mainen, 2003). In total, eight rats were used. Five rats were trained to perform in a reaction time version of the task (Uchida and Mainen, 2003), and the other three rats in a go-signal paradigm (Rinberg et al., 2006) (see Supplemental Experimental Procedures). Three rats (two of them trained with go-signals) were tested on a standardized stimulus set of three odor pairs: (1) caproic acid and citralva, (2) ethyl 3-hexenoate and 1-hexanol, and (3) dihydroxy linalool oxide versus cumin aldehyde (Figure 1B). Each of these odors was diluted 1:10 in mineral oil, and further diluted by filtered air by 1:20 (1:200 total).

Neural Recording

After reaching asymptotic performance in behavioral training, each rat was implanted with a custom-made multielectrode drive (Cury and Uchida, 2010) in the left hemisphere in the aPC (3.5 mm anterior to bregma, 2.5 mm lateral to midline) and a bipolar stimulating electrode in the olfactory bulb (Kashiwadani et al., 1999; Schoenbaum and Eichenbaum, 1995) under anesthesia. Extracellular recordings were obtained using six independently adjustable tetrodes. To monitor sniffing, during drive implantation, a temperature sensor (thermocouple) was implanted in one nostril (Cury and Uchida, 2010; Uchida and Mainen, 2003).

SUPPLEMENTAL INFORMATION

Supplemental Information includes eight figures and Supplemental Experimental Procedures and can be found with this article online at doi:10.1016/j.neuron.2012.04.021.

ACKNOWLEDGMENTS

We are grateful to Haim Sompolinsky for stimulating discussions on population coding. We thank John Maunsell, Markus Meister, Alex Pouget and Rachel Wilson for their valuable comments on the manuscript. We also thank Kevin Cury, Rafi Haddad, Gabriel Kreiman, Eran Mukamel, Alice Wang, and other members of the Uchida lab for discussions. This work was supported by National Institutes of Health Grant DC006104, Cold Spring Harbor Laboratory and Champlimaud Foundation (Z.F.M.); Swartz Foundation, Smith Family New Investigator Award, Alfred Sloan Foundation, Milton Fund and start-up funding from Harvard University (N.U.). N.U. and Z.F.M. designed the experiments and wrote the paper. N.U. performed the experiments. K.M. performed the data analysis and helped writing the paper. N.U. and Z.F.M. helped with the data analysis.

Accepted: April 11, 2012
Published: June 20, 2012

REFERENCES

Averbeck, B.B., Latham, P.E., and Pouget, A. (2006). Neural correlations, population coding and computation. Nat. Rev. Neurosci. *7*, 358–366.

Bair, W., Zohary, E., and Newsome, W.T. (2001). Correlated firing in macaque visual area MT: time scales and relationship to behavior. J. Neurosci. *21*, 1676–1697.

Bhandawat, V., Olsen, S.R., Gouwens, N.W., Schlief, M.L., and Wilson, R.I. (2007). Sensory processing in the Drosophila antennal lobe increases reliability and separability of ensemble odor representations. Nat. Neurosci. *10*, 1474–1482.

Blumhagen, F., Zhu, P., Shum, J., Schärer, Y.P., Yaksi, E., Deisseroth, K., and Friedrich, R.W. (2011). Neuronal filtering of multiplexed odour representations. Nature *479*, 493–498.

Britten, K.H., Newsome, W.T., Shadlen, M.N., Celebrini, S., and Movshon, J.A. (1996). A relationship between behavioral choice and the visual responses of neurons in macaque MT. Vis. Neurosci. *13*, 87–100.

Cang, J., and Isaacson, J.S. (2003). In vivo whole-cell recording of odor-evoked synaptic transmission in the rat olfactory bulb. J. Neurosci. *23*, 4108–4116.

Carey, R.M., and Wachowiak, M. (2011). Effect of sniffing on the temporal structure of mitral/tufted cell output from the olfactory bulb. J. Neurosci. *31*, 10615–10626.

Churchland, M.M., Yu, B.M., Cunningham, J.P., Sugrue, L.P., Cohen, M.R., Corrado, G.S., Newsome, W.T., Clark, A.M., Hosseini, P., Scott, B.B., et al. (2010). Stimulus onset quenches neural variability: a widespread cortical phenomenon. Nat. Neurosci. *13*, 369–378.

Cohen, M.R., and Kohn, A. (2011). Measuring and interpreting neuronal correlations. Nat. Neurosci. *14*, 811–819.

Cohen, M.R., and Maunsell, J.H. (2009). Attention improves performance primarily by reducing interneuronal correlations. Nat. Neurosci. *12*, 1594–1600.

Cohen, M.R., and Newsome, W.T. (2009). Estimates of the contribution of single neurons to perception depend on timescale and noise correlation. J. Neurosci. *29*, 6635–6648.

Cury, K.M., and Uchida, N. (2010). Robust odor coding via inhalation-coupled transient activity in the mammalian olfactory bulb. Neuron *68*, 570–585.

de la Rocha, J., Doiron, B., Shea-Brown, E., Josić, K., and Reyes, A. (2007). Correlation between neural spike trains increases with firing rate. Nature *448*, 802–806.

Dodd, J.V., Krug, K., Cumming, B.G., and Parker, A.J. (2001). Perceptually bistable three-dimensional figures evoke high choice probabilities in cortical area MT. J. Neurosci. *21*, 4809–4821.

Ecker, A.S., Berens, P., Keliris, G.A., Bethge, M., Logothetis, N.K., and Tolias, A.S. (2010). Decorrelated neuronal firing in cortical microcircuits. Science *327*, 584–587.

Franks, K.M., Russo, M.J., Sosulski, D.L., Mulligan, A.A., Siegelbaum, S.A., and Axel, R. (2011). Recurrent circuitry dynamically shapes the activation of piriform cortex. Neuron *72*, 49–56.

Friedrich, R.W., and Laurent, G. (2001). Dynamic optimization of odor representations by slow temporal patterning of mitral cell activity. Science *291*, 889–894.

Gawne, T.J., and Richmond, B.J. (1993). How independent are the messages carried by adjacent inferior temporal cortical neurons? J. Neurosci. *13*, 2758–2771.

Ghosh, S., Larson, S.D., Hefzi, H., Marnoy, Z., Cutforth, T., Dokka, K., and Baldwin, K.K. (2011). Sensory maps in the olfactory cortex defined by long-range viral tracing of single neurons. Nature *472*, 217–220.

Gollisch, T., and Meister, M. (2008). Rapid neural coding in the retina with relative spike latencies. Science *319*, 1108–1111.

Gu, Y., Liu, S., Fetsch, C.R., Yang, Y., Fok, S., Sunkara, A., DeAngelis, G.C., and Angelaki, D.E. (2011). Perceptual learning reduces interneuronal correlations in macaque visual cortex. Neuron *71*, 750–761.

Haberly, L.B. (2001). Parallel-distributed processing in olfactory cortex: new insights from morphological and physiological analysis of neuronal circuitry. Chem. Senses *26*, 551–576.

Hamilton, K.A., and Kauer, J.S. (1989). Patterns of intracellular potentials in salamander mitral/tufted cells in response to odor stimulation. J. Neurophysiol. *62*, 609–625.

Illig, K.R., and Haberly, L.B. (2003). Odor-evoked activity is spatially distributed in piriform cortex. J. Comp. Neurol. *457*, 361–373.

Junek, S., Kludt, E., Wolf, F., and Schild, D. (2010). Olfactory coding with patterns of response latencies. Neuron *67*, 872–884.

Kashiwadani, H., Sasaki, Y.F., Uchida, N., and Mori, K. (1999). Synchronized oscillatory discharges of mitral/tufted cells with different molecular receptive ranges in the rabbit olfactory bulb. J. Neurophysiol. *82*, 1786–1792.

Kazama, H., and Wilson, R.I. (2009). Origins of correlated activity in an olfactory circuit. Nat. Neurosci. *12*, 1136–1144.

Kepecs, A., Uchida, N., and Mainen, Z.F. (2006). The sniff as a unit of olfactory processing. Chem. Senses *31*, 167–179.

Kohn, A., and Smith, M.A. (2005). Stimulus dependence of neuronal correlation in primary visual cortex of the macaque. J. Neurosci. *25*, 3661–3673.

Lee, D., Port, N.L., Kruse, W., and Georgopoulos, A.P. (1998). Variability and correlated noise in the discharge of neurons in motor and parietal areas of the primate cortex. J. Neurosci. *18*, 1161–1170.

Macrides, F., and Chorover, S.L. (1972). Olfactory bulb units: activity correlated with inhalation cycles and odor quality. Science *175*, 84–87.

Margrie, T.W., and Schaefer, A.T. (2003). Theta oscillation coupled spike latencies yield computational vigour in a mammalian sensory system. J. Physiol. *546*, 363–374.

McCollum, J., Larson, J., Otto, T., Schottler, F., Granger, R., and Lynch, G. (1991). Short-latency single unit processing in olfatory cortex. J. Cogn. Neurosci. *3*, 293–299.

Meredith, M. (1986). Patterned response to odor in mammalian olfactory bulb: the influence of intensity. J. Neurophysiol. *56*, 572–597.

Mitchell, J.F., Sundberg, K.A., and Reynolds, J.H. (2009). Spatial attention decorrelates intrinsic activity fluctuations in macaque area V4. Neuron *63*, 879–888.

Miyamichi, K., Amat, F., Moussavi, F., Wang, C., Wickersham, I., Wall, N.R., Taniguchi, H., Tasic, B., Huang, Z.J., He, Z., et al. (2011). Cortical representations of olfactory input by trans-synaptic tracing. Nature *472*, 191–196. Published online December 22, 2010. 10.1038/nature09714.

Nagayama, S., Enerva, A., Fletcher, M.L., Masurkar, A.V., Igarashi, K.M., Mori, K., and Chen, W.R. (2010). Differential axonal projection of mitral and tufted cells in the mouse main olfactory system. Front. Neural Circuits *4*. Published online September 23, 2010. 10.3389/fncir.2010.00120.

Ojima, H., Mori, K., and Kishi, K. (1984). The trajectory of mitral cell axons in the rabbit olfactory cortex revealed by intracellular HRP injection. J. Comp. Neurol. *230*, 77–87.

Parker, A.J., and Newsome, W.T. (1998). Sense and the single neuron: probing the physiology of perception. Annu. Rev. Neurosci. *21*, 227–277.

Perez-Orive, J., Mazor, O., Turner, G.C., Cassenaer, S., Wilson, R.I., and Laurent, G. (2002). Oscillations and sparsening of odor representations in the mushroom body. Science *297*, 359–365.

Perez-Orive, J., Bazhenov, M., and Laurent, G. (2004). Intrinsic and circuit properties favor coincidence detection for decoding oscillatory input. J. Neurosci. *24*, 6037–6047.

Poo, C., and Isaacson, J.S. (2009). Odor representations in olfactory cortex: "sparse" coding, global inhibition, and oscillations. Neuron *62*, 850–861.

Renart, A., de la Rocha, J., Bartho, P., Hollender, L., Parga, N., Reyes, A., and Harris, K.D. (2010). The asynchronous state in cortical circuits. Science *327*, 587–590.

Rennaker, R.L., Chen, C.F., Ruyle, A.M., Sloan, A.M., and Wilson, D.A. (2007). Spatial and temporal distribution of odorant-evoked activity in the piriform cortex. J. Neurosci. *27*, 1534–1542.

Rinberg, D., Koulakov, A., and Gelperin, A. (2006). Speed-accuracy tradeoff in olfaction. Neuron *51*, 351–358.

Schoenbaum, G., and Eichenbaum, H. (1995). Information coding in the rodent prefrontal cortex. I. Single-neuron activity in orbitofrontal cortex compared with that in pyriform cortex. J. Neurophysiol. *74*, 733–750.

Shadlen, M.N., Britten, K.H., Newsome, W.T., and Movshon, J.A. (1996). A computational analysis of the relationship between neuronal and behavioral responses to visual motion. J. Neurosci. *16*, 1486–1510.

Shepherd, G.M. (2004). The Synaptic Organization of the Brain (Oxford: Oxford University Press).

Shusterman, R., Smear, M.C., Koulakov, A.A., and Rinberg, D. (2011). Precise olfactory responses tile the sniff cycle. Nat. Neurosci. *14*, 1039–1044.

Sompolinsky, H., Yoon, H., Kang, K., and Shamir, M. (2001). Population coding in neuronal systems with correlated noise. Phys. Rev. E Stat. Nonlin. Soft Matter Phys. *64*, 051904.

Sosulski, D.L., Bloom, M.L., Cutforth, T., Axel, R., and Datta, S.R. (2011). Distinct representations of olfactory information in different cortical centres. Nature *472*, 213–216.

Spors, H., and Grinvald, A. (2002). Spatio-temporal dynamics of odor representations in the mammalian olfactory bulb. Neuron *34*, 301–315.

Stettler, D.D., and Axel, R. (2009). Representations of odor in the piriform cortex. Neuron *63*, 854–864.

Thorpe, S., Delorme, A., and Van Rullen, R. (2001). Spike-based strategies for rapid processing. Neural Netw. *14*, 715–725.

Uchida, N., and Mainen, Z.F. (2003). Speed and accuracy of olfactory discrimination in the rat. Nat. Neurosci. *6*, 1224–1229.

Uka, T., and DeAngelis, G.C. (2004). Contribution of area MT to stereoscopic depth perception: choice-related response modulations reflect task strategy. Neuron *42*, 297–310.

Wachowiak, M. (2011). All in a sniff: olfaction as a model for active sensing. Neuron *71*, 962–973.

Wehr, M., and Laurent, G. (1996). Odour encoding by temporal sequences of firing in oscillating neural assemblies. Nature *384*, 162–166.

Welker, W.I. (1964). Analysis of sniffing of the albino rat. Behavior *22*, 223–244.

Wellis, D.P., Scott, J.W., and Harrison, T.A. (1989). Discrimination among odorants by single neurons of the rat olfactory bulb. J. Neurophysiol. *61*, 1161–1177.

Wesson, D.W., Carey, R.M., Verhagen, J.V., and Wachowiak, M. (2008). Rapid encoding and perception of novel odors in the rat. PLoS Biol. *6*, e82.

Wilson, D.A. (1998). Habituation of odor responses in the rat anterior piriform cortex. J. Neurophysiol. *79*, 1425–1440.

Zhan, C., and Luo, M. (2010). Diverse patterns of odor representation by neurons in the anterior piriform cortex of awake mice. J. Neurosci. *30*, 16662–16672.

Zohary, E., Shadlen, M.N., and Newsome, W.T. (1994). Correlated neuronal discharge rate and its implications for psychophysical performance. Nature *370*, 140–143.

Neuron, Volume *74*

Supplemental Information

Odor Representations in Olfactory Cortex: Distributed Rate Coding and Decorrelated Population Activity

Keiji Miura, Zachary F. Mainen and Naoshige Uchida

SUPPLEMENTAL FIGURES

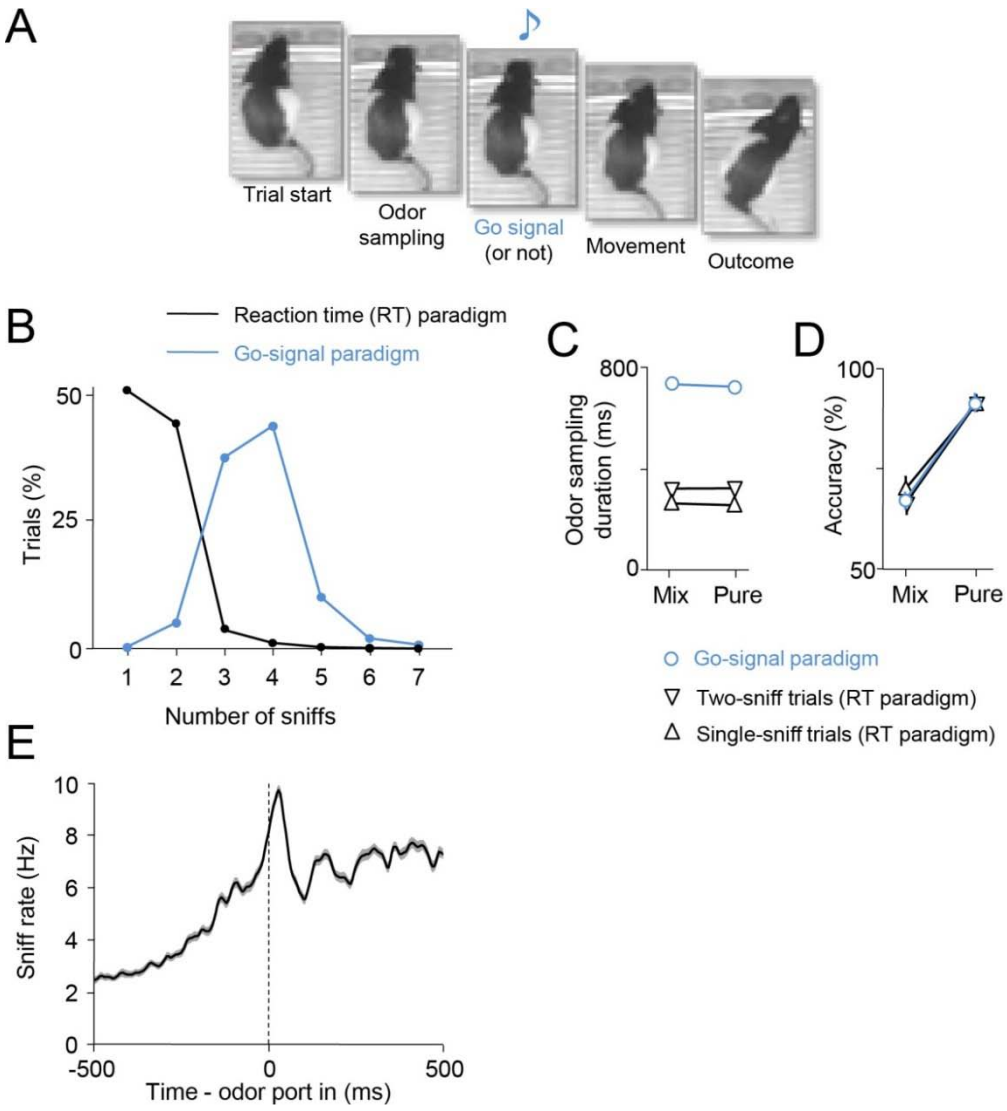

Figure S1, related to Figure 1. Behavioral performance.

A, Schematic of the two behavioral paradigms. In a reaction time (RT) paradigm, the rat was allowed to leave the odor port as soon as they made a decision. In a go-signal paradigm, a pure tone (♪) was played 700 ms after odor valve onset.

B, Histograms of number of sniffs taken during odor sampling period in the reaction time (black) and the go-signal (grey) paradigms.

C, Odor sampling time for different conditions for a rat. ○: trials with go signals. Δ: trials in which rats took one sniff during odor sampling. ∇: trials in which rats took two sniffs during odor sampling.

D, Performance accuracy for different conditions. Same symbols as in **C**. Note that the accuracy was independent of number of sniffs or presence of go-signal (longer odor sampling).

E, Sniff rate as a function of time from the odor port entry for a rat trained in a reaction time paradigm.

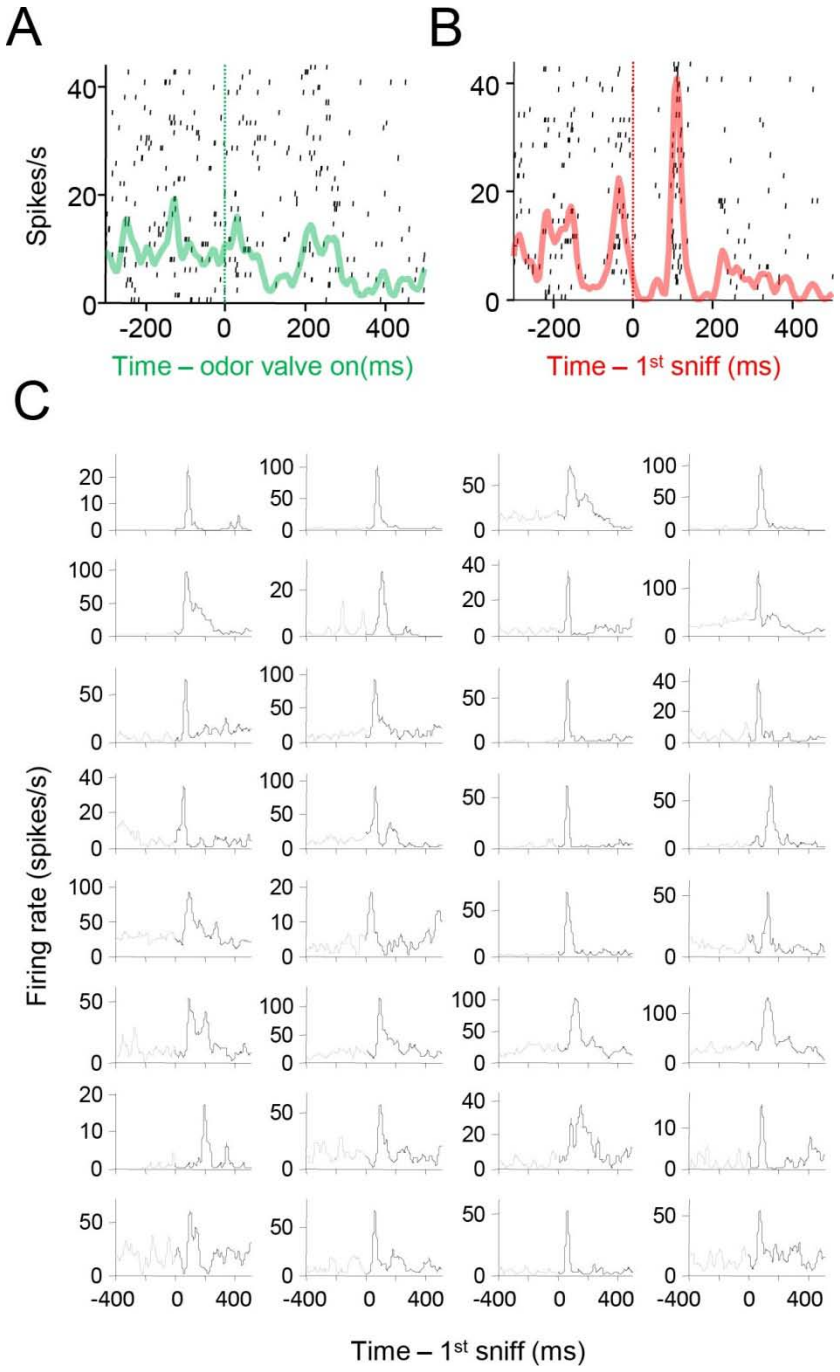

Figure S2, related to Figure 2. Tight locking to inhalation onset and transient responses are common features of aPC neurons.

A & **B,** Activity of an example neuron in the same format as **Figures 2A, B** (N = 47 trials). This neuron responded with the occurrence of 1-2 spikes at the precise latency from sniff onset. This response is only evident when trials were aligned to sniff onset (**B**) but not when aligned to odor valve onset (**A**).

C, Examples of transient odor responses. Peri-event time histograms (PETHs) of spikes for different neurons showing odor responses. Randomly chosen odor responsive neurons are shown. The mean peak

time for these examples is 90.8 ± 34.1(ms) and the mean half width is 33.2 ± 11.2 (ms).

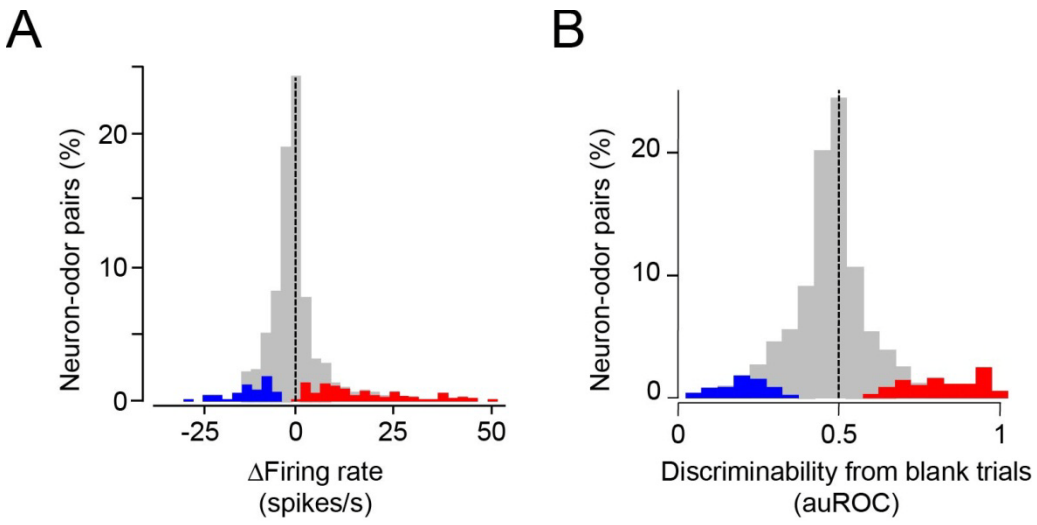

Figure S3, related to Figure 3. Robust odor responses in aPC.
A, Histogram of odor response magnitudes (changes in firing rate during the first sniff cycle). Blue: excitatory, red: inhibitory responses, respectively ($P < 0.05$; Wilcoxon rank sum test).
B, Single neuron response magnitudes characterized by discriminability from blank trials. How accurately an observer can tell odor trials from blank trials in a trial-by-trial basis is quantified by the area under the receiver-operating characteristics curve (auROC). Spike counts in the first sniff (40-160 ms) after odor onset were used. 1: excitatory response with perfect discriminability, 0.5: no discriminability (no response), 0: inhibitory response with perfect discriminability. Colors indicate discriminability that is significantly different from chance performance (0.5) ($P < 0.05$, Wilcoxon rank sum test). Note that single neurons can provide reliable information about the presence of an odor.

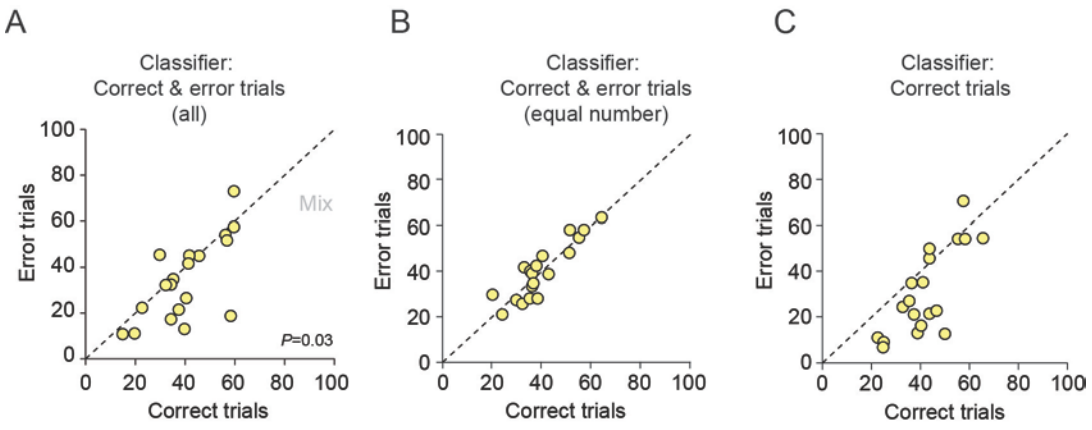

Figure S4, related to Figure 5. Odor decoding accuracy using different sets of correct and error trials for training a classifier.

A, A mixture of all correct and error trials excluding test trials.

B, A mixture of equal number of correct and error trials excluding test trials.

C, Correct trials only (excluding test trials).

Decoding accuracy is higher for correct trials when a classifier was trained by all trials or correct trials only. When the same number of correct and error trials were used for training a classifier, the decoding accuracy matched between correct and error trial. These results suggest that odor responses in correct and error trials are systematically shifted.

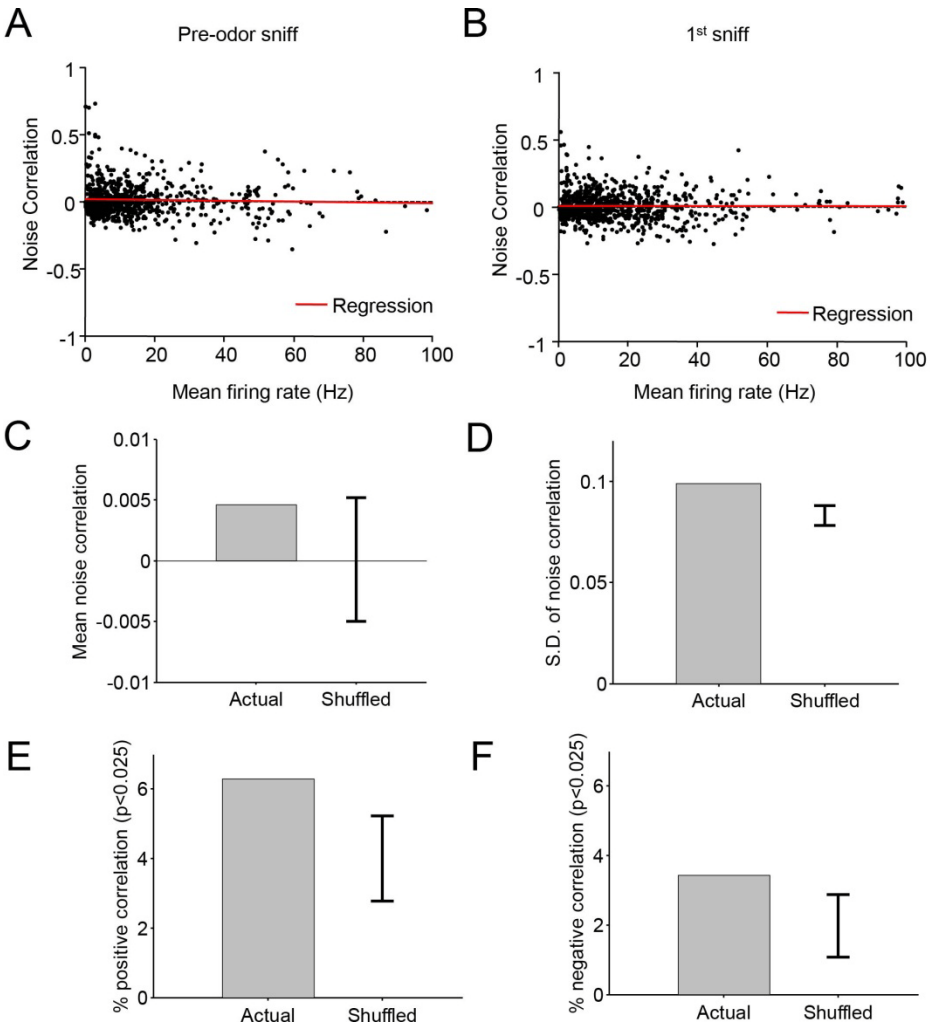

Figure S5, related to Figure 6. Small noise correlations regardless of firing rates of neurons and distribution of noise correlations after trial shuffling.

A & B, Noise correlations as a function of mean firing rates of a pair of neurons. Noise correlations are small regardless of the firing rates. Two task epochs are shown (a: pre-odor, b: first sniff). The slopes of both regression lines (red) are not significantly different from zero ($P > 0.05$).

C, Mean noise correlation for actual and shuffled data (5% confidence interval obtained from 1000 repeats of shuffles). This shuffling analysis was performed in order to estimate the expectation from a population with zero noise correlations but with a limited data set of size matched to ours (**Figure 6A**).

D, Standard deviation of noise correlation for actual and shuffled data. Note that the actual standard deviation is only slightly larger than those obtained after trial shuffling.

E, Fraction of significant positive correlations for actual and shuffled data. Note that the actual fraction of significant correlation is only slightly larger than those obtained after trial shuffling.

F, Fraction of significant negative correlations for actual and shuffled data.

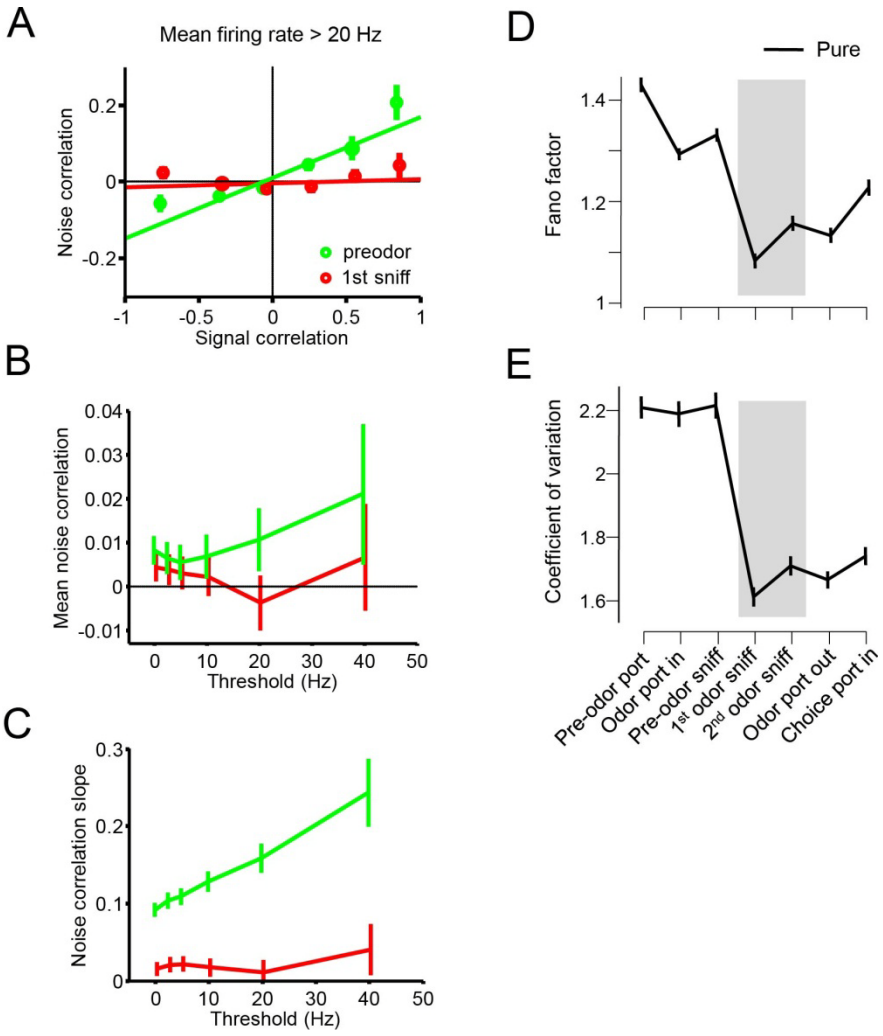

Figure S6, related to Figure 7. Structured noise correlations during pre-odor and decorrelations during 1st sniff are observed regardless of the firing rates.

A, Noise and signal correlations for neurons-odor pairs whose sum of firing rates is higher than 20Hz at the first sniff (threshold = 20 Hz).

B, Mean noise correlation at pre-odor (green) and first sniff (red) periods as a function of threshold firing rates. Only neurons-odor pairs whose sum of firing rates at the first sniff is higher than a threshold are used to compute noise correlations. Threshold = 0 Hz corresponds to the results presented in the main figures.

C, Mean noise correlation slope at pre-odor (green) and first sniff (red) periods as a function of threshold firing rates.

D, E, Spiking variability is quenched by odor stimulation. Fano factor (**D**) and coefficient of variation (**E**) of spike counts in 120ms bins as a function of task epochs. Neural responses aligned by the first sniff after each event were used as in **Figures 7A-C**.

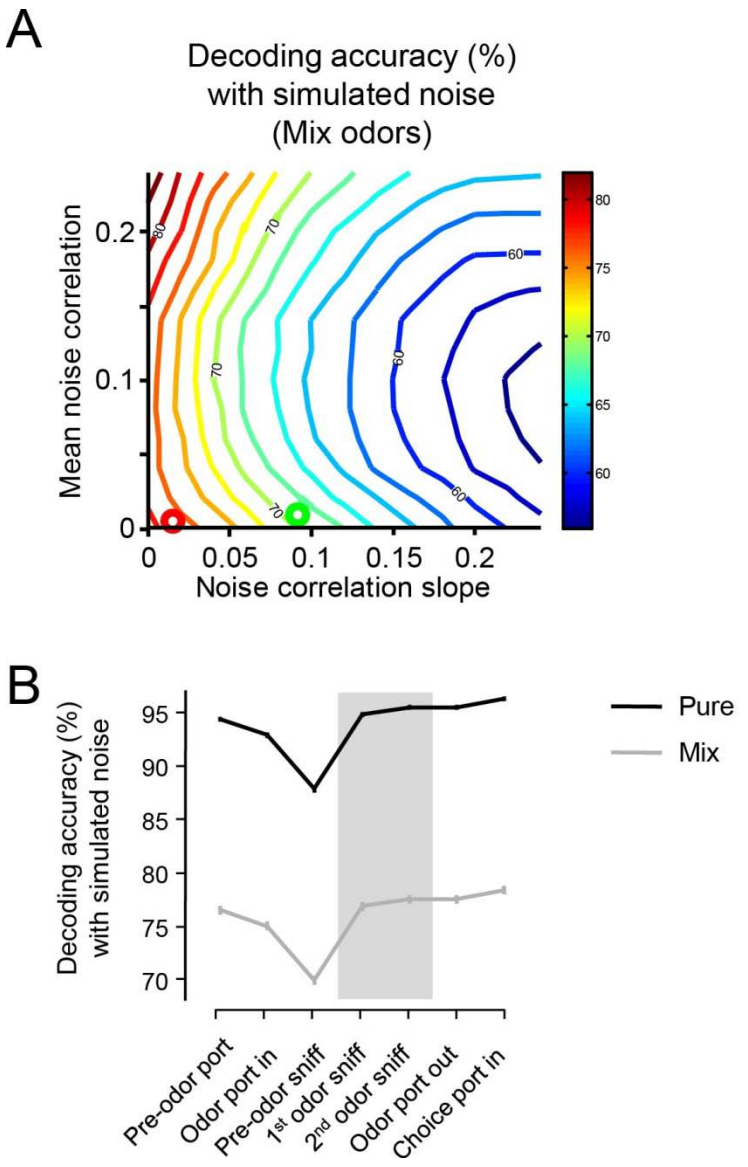

Figure S7, related to Figure 8. Decoding accuracy with induced noise correlation structures observed in different task epochs.

A, Odor decoding accuracy in the presence of simulated noise correlation structures for mixture odor trials. Same format as **Figure 8A** .

B, The decoding accuracy was computed for shuffled data which imitated the mean and slope of noise correlation structures at each task epoch. First, the noise structures were computed at each epoch while the signal correlations were taken from the first sniff period. Then, the decoding accuracy was computed by looking up **Figure 8A** as a table using the linear interpolation.

SUPPLEMENTAL EXPERIMENTAL PROCEDURES

All procedures involving animals were carried out in accordance with NIH standards and approved by the Cold Spring Harbor Laboratory and Harvard University Institutional Animal Care and Use Committee (IACUC). All values were represented by mean ± S.E.M unless otherwise noted. Unless otherwise noted, a nonparametric statistical test, the Wilcoxon rank sum test and a significance level of $P < 0.05$ was used and values are uncorrected for multiple comparisons.

Behavioral task

Eight Long Evans rats (250 g at the start of training) were used. Rats were trained and tested on a two-alternative choice odor mixture categorization task where water was used as a reward as described previously (Uchida and Mainen, 2003). The animals were maintained on a reverse 12 hr light/dark cycle and tested during their dark period. They were allowed free access to food but were restricted to water available during the behavioral session and for 30 minutes after the session. The behavioral setup consisted of a box with a panel containing three ports: a central port for odor delivery and two lateral ports for water delivery.

Rats initiated a trial by entering the central odor-sampling port, which triggered the delivery of an odor with a (uniform) random delay of 0.2–0.5 s (**Figures 1C, S1A**). The odor was available for up to 1 s. In a reaction time version of the task (N = 5 rats), rats could exit from the odor port at any time, and make a movement to either of the two reward ports. Odor delivery was terminated as soon as the rat exited the odor port. Reward was available for correct choices for up to 2 s after the rat left the odor sampling port. Water was delivered with a random delay from entry into the goal port drawn from a uniform distribution [1.0-1.5] s. Rats were first trained with a pair of pure odors and binary odor mixtures in different proportions (68/32, 32/68) where rats were rewarded for choosing the side determined by the dominant odorant. After reaching an asymptotic performance with the first odor pair, rats were trained with the next odor pairs. In addition we used a go signal paradigm (Rinberg et al., 2006b) (N = 3 rats), where rats were further trained to stay in the odor sampling port until an auditory “go” signal delivered 700 ms

after odor port entry. If the subject left the odor sampling port before the go signal, reward was omitted. On average, a behavioral session consisted of 561 valid trials (about 98 minutes).

Behavioral accuracy was defined as the percent correct choices (over the total number of correct and error trials; error trials were defined as trials in which an incorrect response was made, excluding trials in which the rats made no choice). The timings when rats entered or left the ports were signaled by the interruption of the infrared beam caused by the rats' snout into ports. We used port beam break signals to determine the position of the animal during the task with high temporal precision.

Odor stimuli

Odor delivery was controlled by a custom made olfactometer (Uchida and Mainen, 2003). We used relatively low concentration of odorants (dilution factor: 0.05-0.005 achieved by diluting 50 ml/min odorized air in a total of 1000 ml/min clean air stream with further dilution of up to 1:10 in mineral oil for some odorants). All stimuli were randomly interleaved during a session. As a control, we also included "blank" trials in some sessions in which air stream through a filter containing no odorants was activated. Rats were rewarded randomly (P = 0.5) at either side of reward ports. After some training, rats made choice movements consistently after hearing a valve click sound with slightly longer reaction times (587 ± 21 ms, 2.59 ± 0.12 sniffs) than odor trials (372 ± 3 ms, 1.25 ± 0.02 sniffs).

Three rats (two of them trained with go-signals) were tested on a standardized stimulus set of three odor pairs: (1) caproic acid and citralva, (2) ethyl 3-hexenoate and 1-hexanol, and (3) dihydroxy linalool oxide vs. cumin aldehyde (**Figure 1B**). Each of these odors was diluted 1:10 in mineral oil. For each pair, we used four complementary mixture ratios (100/0, 68/32, 32/68, 0/100). The data set with this condition consisted of 36 experimental conditions (3 rats x 3 odorant pairs x 4 mixture ratios). Each of the three rats was tested in four to nine sessions (one session per day), yielding a total of 10,668 trials during recording. This data set contained 179 neurons and was used for the classification success analysis. An additional five rats were tested using different combinations of odors (three to four mixture pairs per session) to examine the basic response properties can be generalized to more odors. The odors used in these experiments

are 5-methyl-3-hexen-2-one, meta-, para-cresol, pentyl acetate, benzaldehyde, anisole, (S)-(+)-carvone, acetophenone, alpha-farnesene and the above six odorants. This data set contained 281 neurons and was used for other analyses that did not require a fixed set of odors in combination with neurons with a fixed odor panel (**Figures 2C, 3B**). The total data set contained 460 neurons from 48 sessions (8 rats).

Analysis of respiration pattern

To monitor sniffing, during drive implantation, a temperature sensor (0.005" Teflon-coated thermocouple, Omega) was implanted in one nostril (Uchida and Mainen, 2003). Respiration patterns were monitored as a temperature change in the nasal cavity as described previously (Kepecs et al., 2007; Uchida and Mainen, 2003). Signals from nasal thermocouple were amplified, filtered between 0.1 and 475 Hz and digitized at 2,000 Hz. For analysis, voltage signals were further low-pass filtered (< 50 Hz). Onset of inhalations and exhalations were identified as local maxima and minima of the signals semi-automatically using custom software.

We excluded the trials with partial inhalations where odorants were delivered in the middle of the inhalation cycle. A criterion "pre-odor exhalation onset < odor onset + 50ms < first inhalation onset" was used to identify full sniff trials. Odor latency of 50 ms was used based on measurements of odor delivery timing using photoiodization detector (PID). The results presented in this paper are not sensitive to this value but the chance-level hit rate in the classification analysis before odor onset supports this estimate (**Figures 5B**).

Neural recordings

After each animal reached an asymptotic performance in behavioral training (3-4 weeks), each rat was implanted with a custom-made multielectrode drive (Cury and Uchida, 2010; Feierstein et al., 2006) in the left hemisphere in the aPC (3.5 mm anterior to bregma, 2.5 mm lateral to midline) under anesthesia (ketamine/medetomidine, 60/0.5 mg/kg, i.p.). A stimulation electrode (a pair of tungsten electrodes, ~150 kΩ) was implanted in the middle of the OB ipsilateral to the recoding site (1.5 mm in depth). Rats were allowed to recover for 5 to 7 days before resuming

water restriction and starting the recordings. Extracellular recordings were obtained using six independently adjustable tetrodes (impedance: 300-600 kΩ). Before starting recordings, animals were retrained to reach similar accuracy levels as those achieved before surgery (>90% correct for pure odors). During this period, electrodes were advanced ventrally to the aPC over 4-7 days. Recordings were obtained for 1–2 weeks with electrode depths adjusted on each recording day so as to sample an independent population of cells across sessions. Neural and behavioural data were synchronized by acquiring time-stamps from the behavioural system along with the electrophysiological signals. Data acquisition was performed using the Cheetah system (Neuralynx, Tucson AZ). Electrode placements were estimated by depth and local field potentials evoked by OB electrical stimulation (approximately 50 μA, 100 μsec) (Haberly, 1973). Recording location was further confirmed by post-hoc histological examination.

Spike sorting and neuron types

Spike waveforms were collected by filtering between 600 and 6,000 Hz and saving 1 ms waveforms triggered by a simple threshold. Single units were isolated offline by manually clustering spike features (peak amplitude, energy and principle components) derived from the sampled waveforms using MClust software (written by A.D. Redish). Although we attempted to sample independent populations of units each session, putatively identical units (based on the similarity of the waveforms) were sometimes encountered. Duplicate units were excluded from the population analysis, but the results were not affected by the inclusion of all units. As in other cortical areas, neurons could be classified into two categories: wide-spiking (width > 0.2 ms) and narrow-spiking neurons (width < 0.2 ms). The width was determined as the time between a peak and a trough of the mean spike waveform. About 6 % (29) of recorded neurons fell into the category of narrow-spiking neurons. Overall, aPC neurons had spontaneous firing rates of 6.15 ± 9.01 Hz (mean ± S.D.). Spontaneous firing rates of wide-spiking neurons were significantly lower than those of narrow-spiking neurons (4.95 ± 6.32 Hz; 24.8 ± 20.1 Hz; mean ± S.D., respectively). Both categories of cells were included in the analyses but exclusion of narrow spike neurons did not affect the main conclusions.

Single neuron analysis

In order to obtain instantaneous firing rates (e.g. for Peri-event time histograms, PETHs), spike events were convolved with a Gaussian filter (S.D.: 7.5 ms) (**Figures 2A-B, 4A, 5E, S2**). To obtain peak timing of odor responses (**Figure 2D**), the PETHs of 243 neuron-odor pairs that showed peak responses > 15 Hz and > 5 S.D. above baseline firing (blank trials) were analyzed. To quantify transience of odor responses, we also obtained the temporal half width from the same neuron-odor pair (**Figure 2E**). The temporal half width was defined as the duration of the time window at which the firing rate was above the half of maximum firing rate from the baseline firing rates.

Because previous studies in the olfactory system suggested that neural responses can be modulated by behavioral context (Cury and Uchida, 2010; Kay and Laurent, 1999; Rinberg et al., 2006a), comparisons were made against "blank" trials (see above). For example, to obtain the number of odor-responsive neurons, comparisons were made using spike counts in a sniff cycle in odor trials against that in a corresponding sniff cycle in blank trials (**Figures 3A, C, D, S3**). We also used pre-odor sniffs (a full sniff cycle immediately before odor onset) as a reference in some cases. These two methods produced essentially similar results. The time window for a sniff cycle was defined as 40–160 ms from inhalation onset (a 120 ms window with 40 ms delay) unless noted otherwise. A 40 ms delay was used because obvious neural responses typically did not occur before 40 ms from inhalation onset although the results did not depend critically on the length of the delay. A 120 ms window was used because the duration of most sniffs are longer than 120 ms (< 8.3 Hz) (Kepecs et al., 2007). For example, odor tunings at the first sniffs were computed based on the numbers of spikes between 40 ms and 160 ms after the inhalation onsets (**Figures 3, S3**). The same window for corresponding sniff periods was used for the classification analysis (**Figures 5A, D, G, 8, S4**), signal and noise correlations (**Figures 6, 7, S5, S6A-C**), Fano factors (**Figures S6D, E**) and sparseness (see Supplementary Experimental Procedures).

Classification success (decoding) analysis

To examine information contents in ensemble activity, we applied a decoding approach (Cury and Uchida, 2010; Hung et al., 2005; Quian Quiroga and Panzeri, 2009). We quantified how

accurately an ideal observer can determine the odor stimulus based on the neural activity on a trial-by-trial basis using a linear classification method. A classification success analysis was used because it is applicable to the size of our data (< 9-17 trials/stimulus). It should be noted that in a classification analysis with finite data set, only part of the information may be retrieved from the data and, therefore, classifiers can only give the lower bound of the information (Duda et al., 2001; Hastie et al., 1995; Narayanan et al., 2005; Quian Quiroga and Panzeri, 2009). However, we could still (1) ask if aPC has at least enough information to explain behavioral performance and (2) explore possible information carrier by comparing information conveyed by different sniff cycles (first, second or last sniff) or different temporal features (spike counts, peak timings or latencies). For a classifier, we mainly used a support vector machine (SVM) with a linear kernel(Hung et al., 2005) and all the plots reported in this paper are based on this method. However, we also tested other classifiers such as a classifier based on a linear discriminant analysis, multilayer perceptrons, and SVM with nonlinear kernels. This confirmed that the main conclusions were not affected by the choice of classifiers.

We used a toolbox in MATLAB (Osu-SVM package) for analyses using a SVM. A matrix containing concatenated firing rates for each trial and each neuron was the input to a classifier (the dimension of the matrix is the number of neurons by the number of trials). To avoid over-fittings, a cross-validation method (the leave-one-out method) was used for calculating the hit rate of odor discrimination. To compute a classification success rate for a given condition, we repeated random sampling of a subset of neurons from the data set 500 times and obtained the average classification success rate (**Figure 5A**). For the analyses of time course (**Figure 5B**), a classifier was trained and tested at each time point (a 50 ms window moved in 5 ms time steps). Classification success analyses were applied to the main data set with the fixed three pairs of odors (six pure odors and six binary mixture odors, three rats, 179 neurons). We used six labels (odor categories) such that a mixture odor belongs to the odor category based on the dominant component. Note that the chance classification performance level is 16.67% (=1/6) with 6 odors.

In order to test whether fine temporal patterns within a sniff cycle convey odor information, we first extracted fine temporal features including (1) latency to the first spike from inhalation onset or (2) peak timing of firing in sniff cycle from the spike trains using the following methods. The timing of peak firing for each trial was identified as the timing of the maximum firing rate within

a window [40-240 ms] in the PETH calculated as above (using a Gaussian filter of 7.5 ms S.D.). The latency of responses was defined as the timing of the first spike within a window [40-240 ms] for each trial. When there is no spike, a random number was assigned to the peak time and latency from a uniform distribution over [40-240 ms] to ensure that the peak time and latency are as independent from spike counts as possible. A matrix containing these temporal firing features was used as an input to a linear classifier and information contents were estimated from classification success rates as described above. The speed with which spike trains convey odor information using different coding schemes was compared as follows (**Figures 4F**). For a given coding scheme (rate, latency, peak or their combinations), classification success rates were calculated using a gradually increasing window (40-50, 40-60, 40-80, 40-120, 40-280 ms, etc).

To compare the first, second and last sniffs in a fair manner, the same number of trials was used for the three epochs (**Figure 5D**). The last sniff taken in the odor sampling port can be the second sniff or later. The number of trials per odor was restricted by the minimum number per session (3~11 trials per odor) because we pooled neurons from different sessions.

In order to examine correlations between behavior and neural activity (**Figure 5G-I**), we performed a classification analysis. A classifier was first trained using a mixture of correct and error trials. Classification success rate was then obtained using test trials that are entirely composed of correct or error trials.

All classification analyses except Figure 5G-I were performed after pooling neurons across animals. The basic observations were preserved across neurons although the absolute classification performance differed across animals.

Noise correlations

Noise is defined as the trial-to-trial variability around the mean response under a given stimulus condition. Noise correlation is defined as the correlation coefficient between the noise of two neurons to multiple presentations of a given odor stimulus. To calculate the correlation coefficient, firing rates were transformed into z-scores (mean subtracted and normalized by the standard deviation of responses) for a given odor (Cohen and Newsome, 2008; Huang and

Lisberger, 2009; Zohary et al., 1994). This guarantees that a noise correlation measures only correlations between noises, independently of neurons' mean responses to odors. We applied this analysis to spike counts from a 120 ms window (40-160 ms from inhalation onset).

For pre-odor epochs, we simply calculated the correlation coefficient between pairs of neurons using spike counts without subtracting the mean responses of each stimulus condition. However, we confirmed that subtracting the mean spike count for each stimulus condition produced similar results.

A chi square test of homogeneity showed that the noise correlation computed for a pair of neurons were independent of stimulus condition in 89.3% of the experiments (P>0.05; correlation coefficients were first transformed to Fisher's z to conform normality assumptions). We therefore combined z-scores from different stimulus conditions to calculate a single value of correlation coefficient for each pair of neurons in **Figures 6-8, S5-7**, using the same format as in the previous study(Zohary et al., 1994). Note that the influence of confounding variables such as stimulus strength was removed by converting spike counts to z-scores using the mean and standard deviation for repetitions of each stimulus type.

Noise in the above analyses was estimated as fluctuation around the mean odor responses but such variations in firing may still include systematic fluctuations due to other parameters such as changes in sniffing patterns and animals' states. In this sense, our definition of noise correlations can be regarded as an operational one.

To control for this effect on our estimate of noise correlations, we first used the following regression model for each odor,

$$r = b_0 + b_1 \cdot x_{freq} + b_2 \cdot x_{amp}$$

where r is the firing rate, x_{freq} is the sniff frequency and x_{amp} is the amplitude of sniffing for a given trial. This model allows us to estimate the "mean" response for a given trial taking into account sniff parameters in addition to odors. We then computed noise correlations after subtracting this estimate (r) from the firing rate in each trial. Using this method, we obtained essentially the same results both in terms of the mean and slope of the noise correlations (mean

noise correlation at first sniff: -0.0003 ± 0.0040, noise correlation slope at pre-odor sniff: 0.1125 ± 0.0225).

Other variables that we did not directly measure or control may also systematically affect the neural activity. This includes (1) lingering odors from the previous trials and (2) imagery of particular odors. The first possibility is unlikely because even if we subtracted the mean firing rates conditioned for previous odors, we obtained similar correlations before odor stimulation (as in **Figures 7B, C**). The second possibility is harder to exclude as it is not possible to measure rat's imagery. Thus we cannot exclude the possibility that structured correlations we observed are due to rats' imagery of particular odors on a trial-to-trial basis. Although such correlated firing should not be regarded as noise correlations, this type of activity can have an impact on decoding in a very similar way as structured noise correlations as they can systematically bias animals' estimate of a presented odor.

Although low firing rates may contribute to low noise correlations, we observed no dependence of the magnitude of noise correlations and the number of evoked spikes over a range of rates < 5 to > 100 spikes·s^{-1} (**Figures S5A, B**)(de la Rocha et al., 2007; Kohn and Smith, 2005) and the absence of relationship between signal and noise correlation remained true even when the analysis was restricted to pairs with firing rates > 20 spikes·s^{-1} (**Figures S6A-C**).

Signal correlations

Signal correlation is defined as the correlation coefficient between the mean firing rates of odor response profiles of two neurons. Signal correlation is calculated only for the odor response period (first sniff after odor onset). We estimated signal correlations using 6 pure and 6 mixture stimuli (12 conditions). Given the large dimensionality of potential odor space (Soucy et al., 2009; Wilson and Mainen, 2006), the values of signal correlations may be underestimated. Thus, the positive relation between noise correlations and signal correlations (**Figures 6D, 7C, D**) could be larger. However, the odors used in the present study drive responses over a wide area of the olfactory bulb (Soucy et al., 2009; Uchida et al., 2000) and we speculate that these odors can indicate connectivity to an extent. Our ability to detect the positive relationship between signal and noise correlations during pre-odor period supports the validity of our method.

Effect of noise correlation structures on population coding efficiency

Most of the previous empirical studies that examined the effect of noise correlations on population coding have mainly focused on the mean correlation (Averbeck and Lee, 2003; Bair et al., 2001; Cohen and Maunsell, 2009; Cohen and Newsome, 2008; Constantinidis and Goldman-Rakic, 2002; Gawne et al., 1996; Gawne and Richmond, 1993; Gu et al., 2011; Gutnisky and Dragoi, 2008; Huang and Lisberger, 2009; Lee et al., 1998; Mitchell et al., 2009; Reich et al., 2001; Zohary et al., 1994). However, theoretical studies indicate that it is not the mean correlation but rather the exact structure of noise correlations that is critical in determining the impact of these correlations on the efficiency of population coding (Abbott and Dayan, 1999; Josic et al., 2009; Sompolinsky et al., 2001; Wilke and Eurich, 2002). First, noise correlations are particularly detrimental to population coding when they are higher in neuron pairs with similar stimulus tuning ("structured" or "limited-range" noise correlations)(Sompolinsky et al., 2001; Wilke and Eurich, 2002). Second, when the noise correlations are uniform across the population, they can be beneficial for population coding (Abbott and Dayan, 1999; Sompolinsky et al., 2001).

Because these theoretical studies have made a variety of assumptions on the spiking statistics (e.g. Gaussian noise), it is not completely clear how these theories can be mapped onto empirical data. In order to understand how these theoretical predictions can be mapped onto our data, we performed a simulation-based analysis. Specifically, we introduced arbitrary noise correlation structures on the empirical data and tested how they affect the accuracy of decoding using a linear decoder. To do so, odor response data obtained during the first sniff period was trial-shuffled to generate an arbitrary structure of noise correlations (**Figures 8, S7**). First, a target noise correlation function (NC_{target}) was defined by a linear regression line as a function of signal correlations ($SC_{observed}$):

$$NC_{target} = aSC_{observed} + b,$$

where a and b denote a slope and an intercept, respectively. We randomly chose two trials for a given odor and neuron, and swapped the spike counts from the two trials. If this swap decreased the mean square error between the data and the target regression line, it was accepted. We

repeated the swap 100 times per neuron-odor pair. After 100 shuffling per neuron-odor pair, simulated data reached an asymptote: most swaps are not accepted any more. Note that this swap procedure changes the noise correlations but not the signal correlation or mean odor response profile of any neuron.

Using this trial-shuffled ensemble activity data, we estimated decoding accuracy using the SVM as described above. Note that this method creates only pair-wise correlations and will not generate higher order correlations. The color map in **Figure 8A** was made by smoothing the decoding accuracy obtained for a given slope and mean of noise correlations achieved after trial-shuffling.

SUPPLEMENTAL ANALYSIS

Sparseness

Sparseness of neural responses was quantified using methods previously used to characterize visual and olfactory responses(Perez-Orive et al., 2002; Rolls and Tovee, 1995; Willmore and Tolhurst, 2001). "Population sparseness" (S_P, or response sparseness) is defined for a given odor using the following formula,

$$Sp = \frac{1 - \frac{[\sum_{j=1}^{N} \frac{r_j}{N}]^2}{\sum_{j=1}^{N} \frac{r_j^2}{N}}}{1 - \frac{1}{N}}$$

where N is the number of neurons and r_j is the response. For a response (r_j), we calculated the absolute values of standardized firing rates (z-scores), where the mean firing rate for a given odor was subtracted by the baseline mean firing rate (in "blank trials"), and normalized by the standard deviation. "Lifetime sparseness" (S_L) is calculated for each neuron using the above formula except j corresponds to each odor and N the total number of odors tested. Accordingly, S_P quantifies sparseness of odor-evoked activity (changes from the baseline) across a population for a given odor (0: uniform, 1: sparse). S_L quantifies sparseness of odor responses (specificity) for a given neuron (0: uniform, 1: sparse). Both indices obtained in our data set (S_L: 0.41, S_P: 0.61) indicated relatively higher density of odor responses compared to mushroom body in locusts (S_L: 0.63, S_P: 0.86)(Perez-Orive et al., 2002) and aPC in anesthetized rats (S_L: 0.88, S_P: 0.93)(Poo and Isaacson, 2009) and were comparable to the antennal lobe in locust (S_L: 0.40, S_P: 0.54)(Perez-Orive et al., 2002).

ROC analysis

Odor response magnitudes were characterized in terms of how discriminable odor responses are from firing in blank conditions using the ROC analysis(Dayan and Abbott, 2001; Green and

Swets, 1966). The area under the ROC curve (auROC) characterizes the discriminability of odor trials from blank trials using the activity of a single neuron (**Figures 3A, C, S3B**). We used the spike counts within a 40 - 160 ms window after first sniff onset following odor valve opening as a neural response. The value of 0.5 indicates no response (chance discrimination). Values larger than 0.5 represent excitatory responses (increase in firing), and those smaller than 0.5 inhibitory responses (decrease in firing). One and zero represent perfect discriminability.

Correlations between single neuron activity and behavioral choice

We examined correlation between single neuron activity and behavioral choice using choice probabilities of individual neurons (**Figures 5F**)(Britten et al., 1996). Choice probabilities were computed for each neuron-odor pair. Only mixture trials were used to obtain greater numbers of error trials. Only neuron- odor pairs that met the following two criteria were used: (1) one of the odors activated strongly compared to another odor (responses of a given pair of odors differed by auROC>0.7 or auROC<0.3) and (2) the numbers of correct and error trials were both greater than five. aROC > 0.5 indicates that the animal made choices to the direction associated with the neuron's "preferred odor" more often when the neural response was greater (positive correlation between activity and choice).

Fano factors

To characterize the variability of a spike count to multiple presentations of a given odor stimulus in a manner which is relatively robust against the firing rate change, we used Fano factor (Churchland et al., 2010; Koch, 1999) as a metric. The Fano factor was defined as the variance over the mean of responses to the given odor stimulus and was computed for each neuron-odor pair (**Figures S6D**).

SUPPLEMENTAL REFERENCES

Abbott, L.F., and Dayan, P. (1999). The effect of correlated variability on the accuracy of a population code. Neural Comput *11*, 91-101.

Averbeck, B.B., and Lee, D. (2003). Neural noise and movement-related codes in the macaque supplementary motor area. J Neurosci *23*, 7630-7641.

Bair, W., Zohary, E., and Newsome, W.T. (2001). Correlated firing in macaque visual area MT: time scales and relationship to behavior. J Neurosci *21*, 1676-1697.

Britten, K.H., Newsome, W.T., Shadlen, M.N., Celebrini, S., and Movshon, J.A. (1996). A relationship between behavioral choice and the visual responses of neurons in macaque MT. Vis Neurosci *13*, 87-100.

Churchland, M.M., Yu, B.M., Cunningham, J.P., Sugrue, L.P., Cohen, M.R., Corrado, G.S., Newsome, W.T., Clark, A.M., Hosseini, P., Scott, B.B.*, et al.* (2010). Stimulus onset quenches neural variability: a widespread cortical phenomenon. Nat Neurosci *13*, 369-378.

Cohen, M.R., and Maunsell, J.H. (2009). Attention improves performance primarily by reducing interneuronal correlations. Nat Neurosci.

Cohen, M.R., and Newsome, W.T. (2008). Context-dependent changes in functional circuitry in visual area MT. Neuron *60*, 162-173.

Constantinidis, C., and Goldman-Rakic, P.S. (2002). Correlated discharges among putative pyramidal neurons and interneurons in the primate prefrontal cortex. J Neurophysiol *88*, 3487-3497.

Cury, K.M., and Uchida, N. (2010). Robust odor coding via inhalation-coupled transient activity in the mammalian olfactory bulb. Neuron *68*, 570-585.

Dayan, P., and Abbott, L.F. (2001). Theoretical neuroscience : computational and mathematical modeling of neural systems (Cambridge, Mass., Massachusetts Institute of Technology Press).

de la Rocha, J., Doiron, B., Shea-Brown, E., Josic, K., and Reyes, A. (2007). Correlation between neural spike trains increases with firing rate. Nature *448*, 802-806.

Duda, R.O., Hart, P.E., and Stock, D.G. (2001). Pattern Classification, 2nd edn (New York, A Wiley-International Publication).

Feierstein, C.E., Quirk, M.C., Uchida, N., Sosulski, D.L., and Mainen, Z.F. (2006). Representation of spatial goals in rat orbitofrontal cortex. Neuron *51*, 495-507.

Gawne, T.J., Kjaer, T.W., Hertz, J.A., and Richmond, B.J. (1996). Adjacent visual cortical complex cells share about 20% of their stimulus-related information. Cereb Cortex *6*, 482-489.

Gawne, T.J., and Richmond, B.J. (1993). How independent are the messages carried by adjacent inferior temporal cortical neurons? J Neurosci *13*, 2758-2771.

Green, D.M., and Swets, J.A. (1966). Signal detection theory and psychophysics (New York, Wiley).

Gu, Y., Liu, S., Fetsch, C.R., Yang, Y., Fok, S., Sunkara, A., DeAngelis, G.C., and Angelaki, D.E. (2011). Perceptual learning reduces interneuronal correlations in macaque visual cortex. Neuron *71*, 750-761.

Gutnisky, D.A., and Dragoi, V. (2008). Adaptive coding of visual information in neural populations. Nature *452*, 220-224.

Haberly, L.B. (1973). Summed potentials evoked in opossum prepyriform cortex. J Neurophysiol *36*, 775-788.

Hastie, T., Tibshirani, R., and Friedman, J. (1995). The elements of statistical learning (New York, Springer).

Huang, X., and Lisberger, S.G. (2009). Noise correlations in cortical area MT and their potential impact on trial-by-trial variation in the direction and speed of smooth-pursuit eye movements. J Neurophysiol *101*, 3012-3030.

Hung, C.P., Kreiman, G., Poggio, T., and DiCarlo, J.J. (2005). Fast readout of object identity from macaque inferior temporal cortex. Science *310*, 863-866.

Josic, K., Shea-Brown, E., Doiron, B., and de la Rocha, J. (2009). Stimulus-dependent correlations and population codes. Neural Comput *21*, 2774-2804.

Kay, L.M., and Laurent, G. (1999). Odor- and context-dependent modulation of mitral cell activity in behaving rats. Nat Neurosci *2*, 1003-1009.

Kepecs, A., Uchida, N., and Mainen, Z.F. (2007). Rapid and precise control of sniffing during olfactory discrimination in rats. J Neurophysiol *98*, 205-213.

Koch, C. (1999). Biophysics of Computation (Oxford, Oxford University Press).

Kohn, A., and Smith, M.A. (2005). Stimulus dependence of neuronal correlation in primary visual cortex of the macaque. J Neurosci *25*, 3661-3673.

Lee, D., Port, N.L., Kruse, W., and Georgopoulos, A.P. (1998). Variability and correlated noise in the discharge of neurons in motor and parietal areas of the primate cortex. J Neurosci *18*, 1161-1170.

Mitchell, J.F., Sundberg, K.A., and Reynolds, J.H. (2009). Spatial attention decorrelates intrinsic activity fluctuations in macaque area V4. Neuron *63*, 879-888.

Narayanan, N.S., Kimchi, E.Y., and Laubach, M. (2005). Redundancy and synergy of neuronal ensembles in motor cortex. J Neurosci *25*, 4207-4216.

Perez-Orive, J., Mazor, O., Turner, G.C., Cassenaer, S., Wilson, R.I., and Laurent, G. (2002). Oscillations and sparsening of odor representations in the mushroom body. Science *297*, 359-365.

Poo, C., and Isaacson, J.S. (2009). Odor representations in olfactory cortex: "sparse" coding, global inhibition, and oscillations. Neuron *62*, 850-861.

Quian Quiroga, R., and Panzeri, S. (2009). Extracting information from neuronal populations: information theory and decoding approaches. Nat Rev Neurosci *10*, 173-185.

Reich, D.S., Mechler, F., and Victor, J.D. (2001). Independent and redundant information in nearby cortical neurons. Science *294*, 2566-2568.

Rinberg, D., Koulakov, A., and Gelperin, A. (2006a). Sparse odor coding in awake behaving mice. J Neurosci *26*, 8857-8865.

Rinberg, D., Koulakov, A., and Gelperin, A. (2006b). Speed-accuracy tradeoff in olfaction. Neuron *51*, 351-358.

Rolls, E.T., and Tovee, M.J. (1995). Sparseness of the neuronal representation of stimuli in the primate temporal visual cortex. J Neurophysiol *73*, 713-726.

Sompolinsky, H., Yoon, H., Kang, K., and Shamir, M. (2001). Population coding in neuronal systems with correlated noise. Phys Rev E Stat Nonlin Soft Matter Phys *64*, 051904.

Soucy, E.R., Albeanu, D.F., Fantana, A.L., Murthy, V.N., and Meister, M. (2009). Precision and diversity in an odor map on the olfactory bulb. Nat Neurosci *12*, 210-220.

Uchida, N., and Mainen, Z.F. (2003). Speed and accuracy of olfactory discrimination in the rat. Nat Neurosci *6*, 1224-1229.

Uchida, N., Takahashi, Y.K., Tanifuji, M., and Mori, K. (2000). Odor maps in the mammalian olfactory bulb: domain organization and odorant structural features. Nat Neurosci *3*, 1035-1043.

Wilke, S.D., and Eurich, C.W. (2002). Representational accuracy of stochastic neural populations. Neural Comput *14*, 155-189.

Willmore, B., and Tolhurst, D.J. (2001). Characterizing the sparseness of neural codes. Network *12*, 255-270.

Wilson, R.I., and Mainen, Z.F. (2006). Early events in olfactory processing. Annu Rev Neurosci *29*, 163-201.

Zohary, E., Shadlen, M.N., and Newsome, W.T. (1994). Correlated neuronal discharge rate and its implications for psychophysical performance. Nature *370*, 140-143.